Tribocorrosion Behavior of Metallic Implants: A Comparative Study of CoCrMo and Ti6Al4V in Simulated Synovial Environments

By

Edward Cudjoe

Submitted in Partial Fulfillment of the Requirements

For the Degree of

Master of Science in Engineering

In the

Mechanical Engineering

Program

YOUNGSTOWN STATE UNIVERSITY

August, 2019

Tribocorrosion Behavior of Metallic Implants: A Comparative Study of CoCrMo and Ti6Al4V in Simulated Synovial Environments

Edward Cudjoe

I hereby release this thesis to the public. I understand that this thesis will be made available from the Ohio LINK ETD Center and the Maag Library Circulation Desk for public access. I also authorize the University or other individuals to make copies of this thesis as needed for scholarly research.

Signature:

Edward Cudjoe, Student	Date

Approvals:

Dr. Jae Joong Ryu, Thesis Advisor	Date
Dr. C. Virgil Solomon, Committee Member	Date
Dr. Kyosung Choo, Committee Member	Date
Dr. Salvatore A. Sanders, Dean of Graduate Studies	Date

Abstract

Total joint replacements (TJR's) are used to replace deteriorating hip joints, knees, shoulders, wrists and fingers for millions of people in modern day medicine. They are treatments used for patients with severe cases of arthritis or rheumatism which are mostly common in old-aged people. There was a reported 1.2 million total joint replacement surgeries, primary and revised, across the United States between the years 2012 and 2017. Recent research has pointed out the primary concern with TJR's is the loosening of the prosthetic which further causes destruction of the bone tissue following wear corrosion and failure of the implant. In addition, there were a total of 350 000 total hip replacement surgeries in the U.S between the years 2012 and 2017. The most common type of hip replacements are metal on metal hip replacements. They are preferred because of the less total loss of material being removed from the ball and socket during articulation, low chance of dislocation and reduced chance of fracture. The most common types of metals used in Metal on Metal hip replacements are Cobalt Chromate alloys and Titanium alloys.

Cobalt Chromate alloys were studied by Haynes in 1900's who showed that the basic binary Cobalt Chromate alloy exhibited high strength and low chemical reactivity. Generally, these alloys have high-wear resistance, high strength and modulus of elasticity and high corrosion resistance which makes them useful for orthopedic implants. Titanium on the other hand is useful for orthopedic implants because of its inertness in a biochemical environment with mechanical strengths.

In this thesis, modular Cobalt Chromate (Co-Cr-Mo) and Titanium (Ti6Al4V) alloys were subjected to continuous fatigue contact in a corrosive biochemical environment. The change in the passive layers of these alloys were observed by electrochemical characterizations during small displacement mechanical loading in different pH environments. Namely, Phosphate Buffer Solution (PBS) with a pH of 7.4, Sodium lactate solution which pH of 4 and 2. To further understand chemo-mechanical synergism, and damage recovery behaviors of two different oxides, a Nano-scratch based experiment was carried out in a tribochemical cell. Cyclic reciprocating motions with an alumina sphere was applied with controlled normal load in the solutions. The open circuit potential and potentiostatic polarization were used to measure the

polarization resistance and potential. Changes of electrochemical responses were monitored using the Gamry Potentiometer to quantitatively compare alterations of wear track area, roughness, and oxide thickness on both implant materials during mechanical wear. After thorough investigation, it can be deduced that the formation of oxide layer in the Titanium alloys occurs during fretting, after fretting and in some instances before fretting. CoCrMo however does not re-passivate during fretting but does recover its oxide layer after.

Acknowledgements

I would like to extend my gratitude Dr. Jae Jong Ryu, my advisor for his guidance in this research and knowledge on how to go about handling the few obstacles I came across during this research. I would also like to thank Dr. Park and Dr. Linkous for their support and teaching on electrochemistry. To my committee members, Dr. Choo and Dr. Solomon for their feedback and support. To Yash Trivedi, thank you for your patience in teaching me how to polish and etch my samples, how to calibrate the Nano-indenter machine and Mihir Patel for his knowledge, assistance and support I am very grateful. I would also like to thank Tim Styranec for his help in preparing sodium lactate environment for this experiment.

A huge thank you to my family, especially my parents and Dr. Elvis Cudjoe, and Hicks' for their continued advice and moral support throughout my journey in Graduate school.

List of Figures

List of Tables

Nomenclature

Ti6Al4V	Titanium 6-Vanadium 4-Aluminum
CoCrMo	Cobalt Chromate Molybdenum
TJR	Total Joint Replacement
AJRR	American Joint Replacement Registry
MoM	Metal on Metal
CAD	Computer Aided Design
CAM	Computer Aided Manufacturing
ASTM	American Society of Testing Materials
HCP	Hexagonal Centered Packing
FCC	Face Centered Cubic
CP	Commercially Pure
BCC	Body Centered Cubic
ELI	Extra-Low Interstitial
SCE	Saturated Calomel Electrode
OCP	Open Circuit Potential
PDP	Potentio-dynamic Polarization

Chapter 1: Introduction

1.1 Introduction

Total joint replacements (TJR) are considered to be one of the most successful reconstructive orthopedic surgeries that can be implemented for functional restoration of damaged joints, and become very common due to increase in aging population. According to the American Joint Replacement Registry (AJRR), there were about 1,200,000 (primary and revised surgeries) across the United States between the years 2012 and 2017 for total joint replacement surgeries [1]. They have conducted replacement surgeries on deteriorating hip joints, knees, shoulders, ankles, elbows, wrists and fingers for millions of people in modern day medicine [2]. These are medical treatments used for patients with severe cases of arthritis and rheumatism which are mostly common orthopedic disease in old-aged people [3]. These surgeries are not only common in old-aged people but also amongst athletes due to injuries suffered while playing respective sports. Due to appreciable progress in research involving TJR's over the past decade, it has been pointed out that the primary concern is with the loosening of the prosthetic which is often combined with osteolysis (destruction of bone tissue) following wear, corrosion and fatigue failure of the implant [2]. Though the modular design of joint replacements are mostly due to ease of customization for individuals, the modular interface such as the stem-head interface is continually subjected to wear and corrosion. These bearing components are usually made of ceramics, metals and polymers [4]. The most common type of TJR's are the metal on metal (MoM) joint replacements consisting of three main parts. The ball, stem and shell which are all made of metal alloys. They are of higher preference to other types of materials because of greater mechanical and manufacturing advantages including less total loss of material being removed the ball and socket, low chance of dislocation and a reduced chance of fracture [5]. The most common types of metallic alloys used in MoM joint replacements are Cobalt Chromate (CoCr), Titanium (Ti) and Stainless Steel alloys. Titanium alloys are the most widely used for medical devices and orthopedic implants because of its excellence of inertness in a biochemical environment and superior mechanical strengths. Likewise Cobalt Chromate alloys are being used for the bearing components of joint replacements due to their high stiffness and mechanical strengths with stable chemical responses in human body. In spite of their excellent mechanical and chemical properties, however, a course of daily motions of patients and corrosive

environment surrounding the implant progressively deteriorate the implant surfaces and lead to unexpected failure of the joint. When the mechanical damage process takes place in chemically reactive environments, the combined complexity modifies the damage mechanisms. For example, CoCr alloys manifests superior strength and hardness compared to Ti alloys. Therefore, it has been understood that longevity of CoCr joints is greater than that of Ti joints. However, previous clinical studies and in vitro simulations of Tribocorrosion presented contrary results, thus Cobalt Chromium implant surface showed higher wear rate than that of the titanium implant surface despite Cobalt Chromate's superior mechanical properties [6,7].

1.2 Background

In the world of physics, friction can be defined as a force which opposes relative motion between contacting systems [8]. Though it's a very common force, it is quite complicated in terms of understanding of its nature but can be characterized using a variety of mechanical testing techniques. One of the fundamental characteristics of this force is that the force of friction is parallel to the surfaces in contact and is always in the opposite direction of motion to the contact surface between the interacting surfaces [8]. There are two main types of friction known, i.e. kinetic and static frictions. In a system experiencing kinetic friction, it is observed that the systems in contact move relative to each other with a significant displacement. In a case of static friction, there is no relative motions between the systems in contact [9]. In simple terms when there is no motion between objects, the magnitude of the static friction is $f_s \leq \mu_s N$ and that of the kinetic friction is $f_k = \mu_k N$. As aforementioned, frictional force resists motion between surfaces in contact. This occurs as a result of the roughness of the surfaces in contact [9]. Even in the perfect smooth surface contact the friction is as a result of the attractive forces between molecules making up the objects or surfaces in electrical and/or chemical bonding [8]. The adhesive forces causing this phenomenon also depend on the electronic structures (electron configurations) of chemical components in contact [9]. Adhesion or adhesive forces usually occur as a result of unwanted removal and attachment of wear debris and material compounds between two surfaces. Adhesive wear can be categorized as adhesive wear caused by plastic deformation and cohesion adhesion between two materials. Abrasion on the other hand can simply be defined as the wear down of a material.

Fatigue can be defined as the weakening of a material which is caused by repeatedly applied loads. It is initiated when materials are subjected to cyclic sliding contact loadings which leads to a progressive and localized structural damage [10]. When a material undergoes fatigue loadings, the applied stress is nominally less than yield point and thus there is no warning prior to failure of the materials. However, the repeated shear loadings produce atomic level dislocations and they turn to microscopic cracks. Stress concentrations at the micro crack tips induce localized plastic deformations [11]. Once a crack reaches a critical size, the plastically deformed top surface layer will be separated from the material and subsequently fractures. The fatigue life is also immensely affected by the grain orientations and surface and subsurface flaws. For instance, square holes or sharp corners lead to increased local stresses where fatigue cracks begin. However, round holes and smooth transitions or fillets increase the fatigue strength of the structure [10]. There are different stages of fatigue. They are stage I crack, stage II crack and eventually ultimate failure. These crack initiations are caused by both high and low cycle fatigue [10]. This process begins when cracks nucleate within a material. It happens at either stress concentrated areas in metallic samples or at localized areas with high void density in polymer samples. At stage I crack, it gradually propagates along crystallographic planes where there are high shear stresses. At the peak or critical size of these cracks, they propagate at a high rate during stage II crack growth in a direction perpendicular to the applied force which subsequently lead to the ultimate failure of the material usually in a brittle manner [10]. All this can be summarized as delamination wear which usually occurs in three stages. It occurs from the formation of voids at the near surface of the material being investigated, growth of cracks parallel to the surface which also causes growth of void and the removal of thin long wear particles from the onset of a crack reaching its critical length [11].

Corrosion can be generally defined as the most undesirable type of attack, which allows one to predict the probable life of an equipment with some degree of accuracy [12]. It affects all materials including metals, polymers and ceramics. It results from chemical and/or physical interactions between the material and its surroundings [12]. Metals are distinctive from other materials by a number of favorable properties including ductility, high tensile strength, and resistance to temperature, electrical and thermal conductivity and easy connection and machining [12]. Relevant elements of machinery, aircraft, cars, power plants, precision tools, civil engineering structures and chemical plants are mostly made of metal. However, the continuous

contact at the assembled interfaces of the parts will lead to significant surface wear damage. Most metals and alloys are not thermodynamically stable in contact with the atmosphere and water. [12]. Therefore, the electrochemical instability of metals manifests challenges to design and produce to be used in ambient and reactive environments. In general, corrosion and wear of these systems critically limits the durability and lifetime of elements and machine systems [12]. Engineering have successfully controlled the rate of corrosion for most applications by using adequate preventive means such as material choice, treatment of surface, electrochemical protection and others. This allows metallic objects to satisfactorily fulfill its function over the predicted timeline [12]. Types of corrosion include; uniform corrosion, galvanic corrosion, fretting corrosion, pitting corrosion, inter-granular corrosion, selective corrosion, erosion corrosion and stress corrosion cracking [12].

This thesis project aims to study fretting corrosion of biomedical implants. This is a type of corrosion that occurs when small relative motions at the asperity scale stimulate contacting surfaces in corrosive environment. The damage is caused by applying a repeated shear load which results in plastic deformations or local pits. The electrochemical reaction accelerates corrosion process through the vulnerable area by fretting This typically occurs in clamped joined interfaces such as bolted assemblies and riveted connections [12]. During transportation, contact surfaces exposed to vibration run a risk of undergoing fretting corrosion [12]. The damage takes place at the areas of two highly loaded surfaces that cannot be moved against each other. Fretting fatigue is usually caused by vibration [12]. The protective film on the metal surfaces is removed by the rubbing action and exposes fresh, active metal to the corrosive ambient [12]. The interlocked interface between head and stem of modular hip joints is subjected to the fretting fatigue due to patient's daily motions and the corrosive synovial fluid [13].

The corrosion mechanism in liquids is constituted by some elements of electrochemistry [14]. Electricity flows from certain areas of a metal surface to other areas through a conductive solution, such as sea water. An anode is a corroded portion of a metal surface from which metal ions are released into the solution (electrolyte) [16]. A cathode however is a portion of a metal surface the free electrons migrate in [16].

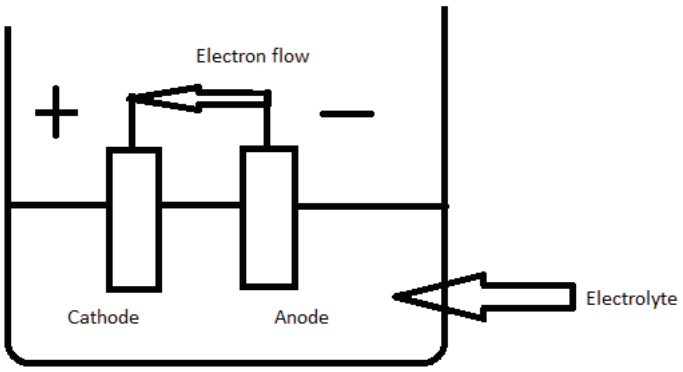

Figure 1: Electron flow in an electrolyte bath

To complete the circuit a conductor is used to join the two pieces of metal outside the solution. An electrolyte is a term used to describe a solution able to conduct electricity due to the presence of ions. These ions are positively or negatively charged atoms or molecules dissolved in the solution. An electrolyte that forms a corrosive environment can be any air-condensed solution, moisture or rain. It can range from a neutral solution to an alkaline or acid [16].

Electrodes is used to describe the anodes and cathodes involved in a corrosion reaction either consisting of two different kinds of metal or located in different areas on the same piece of metal. As stated earlier, the anode (negative electrode) is where corrosion occurs [16].

One of the main causes of metallic corrosion is the electrochemical reactions at the interface between the metal and an electrolyte solution [16]. In a cathodic reaction, a solution species which is often O_2 or H^+ is reduced, which ends up removing electrons from the metal [16]. When these two reactions are in balance, the flow of electric current (electron flow) from each reaction is balanced, and there is no net electrical current [16]. These reactions can occur on a single metal or two different metal sites connected electrically.

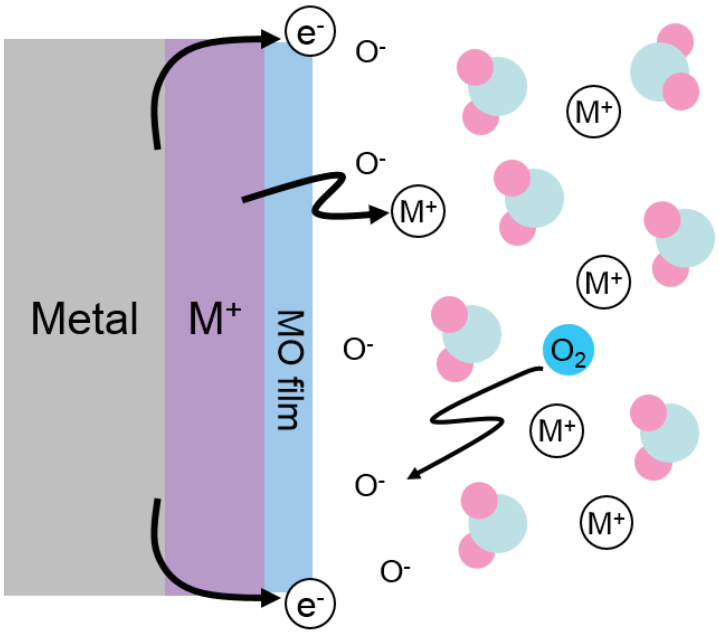

Figure 2: Electrochemistry of metal ion dissolution in liquid

Keeping the anodic and cathodic reactions of a metal in equilibrium is known as the potential of a metal. The current of every half-reaction depends on the electrochemical potential. For instance, if the anodic reaction releases too many electrons in the metal, the excess electrons slow the anodic reaction and increase the cathodic potential subsequently cancelling out the initial perturbation of the system [26]. Open-circuit potential (E_{oc}) is defined as the equilibrium potential of the metal relative to a reference electrode in the absence of the electrical connections in a solution [16]. The most fundamental study of electrochemical corrosion is the open-circuit measurement. Corrosion current (I_{corr}) is the value of either the cathodic or anodic current at open-circuit potential [16]. There are certain system parameters that affect the corrosion current and rate. These parameters include, type of metal, composition of the solution, metal history, temperature, movement of the solution [16].

Also, in order to understand details in electrochemical responses a potentiostat controller is employed. The potentiostat allows to control potentials of a metal and measure the corrosion current to determine electrochemical reactivity of the metal piece in the surrounding solution. A

potentiostatic polarization is the measure of current across the surface of the metal over a period of time. Polarizing a sample means forcing the electrical potential of the metal surface in a solution away from an open circuit potential. The current (response) of the sample is measured as it is polarized. This response is used to develop a model of the samples corrosion behavior [16].

Total joint replacements (TJR's) also sometimes referred to as prosthetic implantation are used to replace deteriorating hip joints, knees, shoulders, ankles, elbows, wrists and fingers for millions of people in modern day medicine [1]. These prosthetic implantations are treatments used for patients with severe cases of arthritis or rheumatism which are mostly common in old-aged people [2]. Surgeries involving total joint replacements are also very common amongst athletes due to injuries suffered while playing sports [2].

As aforementioned, the American Joint Replacement Registry (AJRR) reported about 1,186,955 (primary and revised surgeries) total joint replacement surgeries across the United States between the years 2012 and 2017 [3], Hence the need to research is obvious to study the effect of the implants on biological systems of human and animals. Due to appreciable progress in research of TJR's over the past decade, it has been pointed out that the primary concern is the loosening of the prosthetic implants caused by periprosthetic osteolysis (destruction of bone tissue) following progressive surface damage by wear and corrosion [1]. Though the modular design of joint replacements are mostly used due to ease of anatomic customization for individuals, the modular interface such as the stem-head interface is continually subjected to wear and corrosion. These modular components are usually made of ceramics, metals and polymers [4]. In the US between the years 2012 and 2017, there were a total of 350,000 total hip replacement surgeries. Recently, successful metallic hip joint prosthetic surgeries have been reported. The metal-on-metal (MoM) hip replacements consist of three main metallic parts including the ball, stem and acetabular cub. This MoM hip replacements have been preferentially employed because of their mechanical excellence resulting in less total loss of material being removed from the ball and socket during articulation, low chance of dislocation when the femur slips out of its socket in the pelvis and a reduced chance of fracture [5]. The most common types of metallic alloys used in MoM hip replacements are stainless steels, Cobalt Chromate alloys and Titanium alloys. Therefore, this research focuses on mechanical and chemical responses of metallic implant materials used in total hip replacement surgeries.

Bioimplants are made from a variety of materials that must be physiologically compatible in the human body. Generally, biomaterials are natural or synthetic materials used in the replacement to improve functions and support the bone structures. They replace living tissues and organs such as heart valves, vessels, joints and others. As they have to conduct biological functions instead of the original organs and tissues, biological and physiological stability at the implant-tissue interfaces is very critical. In some situations, biomaterials are also required to be degradable or naturally-dissolving to disappear from the entity after its function has been fulfilled [6]. Another application of biomaterials is to deliver medications to targeted parts using dissolvable capsules for carrying drugs toward the desirable area in the body. Bone fracture fixture in the form of scaffold structure has been used to support and repair damaged bone tissues. Such implantable materials are made from three main materials, i.e. metals, ceramics and polymers or composites [6].

1.2.1 Metallic Implants

The use of metallic materials for prosthetic implants can be followed back to the 19th Century, paving the way to the period when the metal industry started to expand amid the Industrial Revolution [17]. The development was driven primarily by the requirements for bone repair approaches, usually internal fracture fixation of long bones. However, there were almost no success in attempts to implant metal devices, such as spinal cables iron, gold or silver bone pins, were successful until Lister's aseptic surgical technique was created in the 1860s [17]. Since that period, metallic materials have played a major role in orthopedic surgery in most orthopedic devices, temporary and permanent implants. Even though a majority of metals and alloys that can be produced in industry, only a select few are bio-compatible and can be an implant material for long-term success [18]. Some of the metallic implants include; Stainless Steels, Titanium based and Cobalt based alloys [17].

In the chemical field, metals are combined with other elements, as metal oxides in the earth's crust in mineral form. These mineral deposits are extracted to supply ore suitable for further processing into pure metal or various alloys. Certain mines in the United States, mainly the South-Eastern parts yield sands containing quartz with deposits of zircon, titanium and iron minerals [17]. Titanium metal can be extracted from rutile using a few methods, one of which involves treating the ore with chlorine to make titanium tetrachloride liquid and then treated with

magnesium or sodium to produce magnesium or sodium chlorides and bulk titanium (Kroll Process) [19, 20]. The titanium bulk produced after this method is usually of low purity. Depending on the level of purity desired, further refinement is done by using vacuum furnaces, re-melting and other additional steps [19]. These steps are important in the production of titanium with the appropriate properties. For instance, commercially pure titanium varies in oxygen by only tenths of a percent. These differences can affect the mechanical properties such as yield, tensile, and fatigue strength of the titanium alloy. The final raw metal product yields some type of bulk form, ingots which are supplied to metal manufacturers [19]. For a multicomponent metallic implant alloy, the raw metal product is usually processed further, chemically and physically, to produce an alloy that meets certain chemical and metallurgical specifications.

Preliminary fabrication and final forms of the orthopedic device is obtained from the raw metal product. The final geometry of the implant, costs of alterative fabrication methods, forming and machining properties of the metal, dictate the specific steps required [20]. Investment casting, forging, conventional and computer-based machining, powder metallurgical processes, and a range of grinding and polishing steps are among the fabrication methods. These manufacturing methods are required because not all the alloys can be manufactured the same way, even economically. A typical example is cobalt-based alloys. These alloys are extremely difficult to machine via conventional methods into the complex shapes of some implants. Hence, many of them are frequently shaped into the desired forms by investment casting [20]. Unlike cobalt-based alloys, titanium is relatively difficult to cast so it is frequently machined. The surface of the implant is then treated using applications of macro or microporous coatings or the deliberate production of certain degrees of surface roughness. The full understanding of the properties of each alloy in terms of microstructure and processing is dependent on the knowledge of the chemical and crystallographic identities of the phases, the relative amounts, distribution and orientation of theses phases and the effects of the phases on properties [20].

- **Cobalt-Based Alloys**

In 1709, Haynes studied Cobalt Chromium alloys and showed that the basic binary CoCr alloy exhibited high strength and low chemical reactivity, and the addition of Molybdenum (Mo) or Tungsten (W) increased the strength of the alloy significantly [21] Generally, CoCr alloys

have high-wear resistance, high strength, high modulus of elasticity and high corrosion resistance. Its possession of such properties is what qualifies its usefulness in orthopedic implants. The alloys were initially used as dental alloys and were later used for orthopedic implants. Due to the success rate of these alloys, they are continually used in many current orthopedic implants such as total hip replacement and total knee replacement [21]. Even though CoCr alloys are used for medical implants because of its high performance, it remains a problem because of its degradation due to wear and corrosion. The damage of implants due to wear and corrosion is known to cause bone destruction (osteolysis) and inflammation to human cells.

CoCr alloys are known to have high corrosion resistance. This can be attributed to the presence of a spontaneously formed thin passive oxide film on the surface under normal conditions. This passive film is usually thin. To put it into perspective, it is a few nanometers thick and is able to isolate the reactive base metal from the surrounding solution and becomes a kinetic barrier to active metal dissolution reactions [22, 23]. The oxide film however loses its protection to corrosion when there is abrasion or other oxide disruption processes like mechanical wear (fretting) on the surface of the CoCrMo alloy [22, 23]. Once there is abrasion of the oxide film, the corrosion rate of base metal increases during repassivation. Also corrosion debris and metal ions generated are usually associated with adverse tissue relations [22, 23], adverse reaction to metal debris [24, 25]. Recent research has proven that high early failure rate of hip implant has been directly linked to fretting corrosion of modular taper interfaces. CoCrMo has been involved in many cases. Therefore, the passive oxide film plays an important role in determining the fretting corrosion susceptibility of CoCrMo alloy [24, 25]. Though oxide films aid in the resistance of corrosion of CoCrMo alloy under normal non-fretting conditions, they are not inert.

Some examples of cobalt-based alloys include American Society for Testing Materials (ASTM) F75 and F90 also known as Haynes-Stellite 21 and 25 respectively, forged Co-Cr-Mo alloy (ASTM F799), ASTM standard F1537 and multiphase (MP) alloy MP35N (ASTM F562) [14]. Some alloys are identical in composition, F75 and F799 are quite identical about 58-70% Co and 26-30% Cr. The main difference is how they are processed [14]. The ASTM F1537 alloy is what was used for this research.

Table 1: Mechanical Properties of ASTM F1537 CoCrMo alloy

Material	Yield Strength (MPa)	Ultimate Strength (MPa)	Hardness (HRC)
CoCrMo (F1537)	958	1338	45

- **Titanium Based Alloys**

Titanium is an element with a low density, approximately 60% of the density of iron and about half the density of cobalt that can be increased in strength by alloying and deformation processing [24]. Once pure titanium experiences an allotropic transformation (approximately 855 ˚C), it changes from a hexagonal close packing phase (HCP) to a body centered cubic phase (BCC). Titanium alloys can be categorized into four classes based on their microstructure after processing. They are α-alloys, near α-alloys, α-β alloys and β alloys [26]. In comparison to other alloys such as cobalt chromium, titanium is higher in specific strength (strength/density) but inferior in tribological properties [26]. Titanium alloys are used as biomaterials due to its low modulus, high biocompatibility and enhanced corrosion resistance unlike cobalt chromium alloys [26]. When it comes to the design of titanium alloys, the main concern are the mechanical properties. This is because the matrix element of titanium is already corrosion resistant [26]. Alloying surfaces of titanium sensitively impacts the transformation temperature between α-HCP and β-BCC. These are grouped into α or β stabilizing additions, depending on the change in the α/β transition temperature [27]. Elements such as oxygen, nitrogen and carbon (interstitial elements) are strong α stabilizers which raise transformation temperature when the solute content increases. On the other hand, hydrogen is considered a strong β stabilizer because it decreases the transformation temperature with increasing solute content [27]. Titanium is a unique metal because of its high solubility of oxygen and nitrogen. Because of this, heating titanium in air high temperatures yields oxidation (solid solution hardening of the surface) also sometimes known as air contamination layer, blemishes the fatigue strength and ductility, such that it must be removed (machining or chemical milling) before being implanted [27]. Aluminum is also a strong α stabilizer. Unlike α titanium, β titanium has more elements solubilized in it. These elements (β stabilizer) are chosen because they do not form intermetallic compounds with titanium and vice versa [27]. Transition metals such as vanadium, molybdenum, chromium, iron, copper, nickel, palladium, cobalt and manganese are used to form eutectoid systems. These

elements are usually added to alloys together with one or more of the β isomorphous elements to stabilize the β phase and prevent the formation of intermetallic compound, during thermo-mechanical processing, heat treatment, or service at elevated temperatures [27]. Vanadium, molybdenum, niobium, chromium, iron and silicon are the most frequently used β stabilizing elements [28]. Because chromium, iron and other compound formers are β stabilizers, improve hardenability and respond to heat treatment, they are sometimes used in β rich, α-β alloys or in β alloys [28]. These elements have significant solubility in both α and β phases but can lower the α/β transformation temperature very slightly, and then increase it again at higher concentrations [28]. Alumina, tin and zirconium are commonly used together in and near-α alloys. In α–β alloys, these elements are distributed approximately equally between α and β phases. Almost all commercial titanium alloys contain one or more of these three elements because they are soluble in both α and β phases, and particularly because they improve creep strength in α phase [28]. The most common titanium alloys used in making implants are commercially pure (CP) titanium (ASTM F67) and extra-low interstitial (ELI) Ti6Al4V alloy (ASTM F136) [28]. Focus will be on ELI Ti6Al4V (ASTM F136). The ELI Ti6Al4V is an alpha-beta alloy, with a microstructure dependent upon heat treatment and mechanical working [28].

Table 2: Mechanical Properties of ASTM F136 Ti6Al4V alloy

Material	Yield Strength (MPa)	Ultimate Strength (MPa)	Hardness (HRC)
Ti6Al4V (F136)	924	1000	33

1.2.2 Ceramic Implants

Ceramics are created from a wide range of inorganic/nonmetallic compositions [21]. They are mainly oxides, but they can be carbides, nitrides, borides and silicide as well. Ceramics can be single compounds or various compounds mixtures [29]. They have vas mechanical and physical properties but known to be hard and brittle. The brittleness of ceramics is as a result of the processing and preparation. These flaws result in premature failure of ceramic materials [30]. In the medical field, ceramics, glasses and glass ceramics are used to create chemical ware, diagnostic instruments, thermometers, tissue culture flasks and eyeglasses.

Ceramics are also used in the dental field as restorative materials such as dentures and glass-filled ionomer cements [30]. They are used in the production of prostheses for joint replacement in orthopedics and for bone reconstruction in osteosynthesis [30].

1.2.3 Polymers/Composites Implants

Composite is a word that means "consisting of two or more noticeable parts. [29]" Materials such as metal alloys and polymeric materials can all be classified as composite materials because they consist of different and clear atomic groupings at the atomic level [29]. At the microstructure level, a metal alloy such as plain carbon steel containing ferrite and pearlite may be referred to as a composite material because ferrite and pearlite are clearly visible components when viewed under the microscope [29]. Bones and tendons can also be referred to as composite with several levels of hierarchy at the molecular level. A composite as a biomaterial is a material consisting of two or more chemically distinct constituents, on a macroscale, with a distinct interface separating them [29]. These such characterized composites have one or more discontinuous phases embedded within a continuous phase [31]. In comparison, the discontinuous phase (reinforcing material) is known to be stronger and harder than the continuous phase (matrix) [31]. The properties of composites are dependent on the properties of their constituent materials, their distribution and content, and the interaction among them [31]. The composite properties may be the volume fraction sum of the properties of the constituents, or the constituents may interact in a synergistic way due to geometrical orientation so as to provide properties in the composite that are not accounted for by a simple volume fraction sum [31]. Specifying the constituent materials and their properties is one way of describing a composite material along with specifying the geometry of the reinforcement, concentration, distribution and orientation [32]. These materials are a created to provide desired mechanical properties such as strength, stiffness, toughness, and fatigue resistance [32]. It is therefore natural to study composites which have a common strengthening mechanism together. This strengthening mechanism is dependent on the geometry of reinforcement. This allows for easy classification of composite materials based on the geometry of reinforcement [32].

With respect to this classification, the distinctive feature of a particle is that it is non-fibrous in nature. It is approximately equiaxial irrespective of its shape [32]. A fiber has a length that is much larger than the cross-sectional dimensions and sometimes particle-reinforced composites

are called particulate composites. Fibrous composites are reinforced fiber composites. A laminate is a composite structure which is created by stacking laminae of fiber composites oriented to produce a structural element [32]. The characteristics, number and orientation of laminae are made to match specific design requirements.

In general, fibers are more mechanically effective than particles, and polymer-fiber composites have high stiffness and strength comparable to those of metals. In comparison, particle-reinforced composites are isotropic while fiber-reinforced composites are anisotropic [33]. When a composite material implant fails, it exposes fibers or particles to the surrounding biological environment. Due to idrothermal aging or stresses exceeding the interface strength, failure in composites is pioneered by failure of the interface between filler and matrix [31]. Method of sterilization can play an important role. Like all biomaterials, the problem of tissue response to the composite is important. With the composition of two or more materials, composites provide augmented probability of causing adverse tissue reactions [32]. The fact that one reinforcement has cellular dimensions always opens the possibility of cellular ingestion of particulate debris, which can either lead to the production of tissue-lysing enzymes or transport to the lymph system [34]. While durability and biocompatibility in a composite medical device can be considered important problems, composites offer unique advantages in terms of design and manufacturing [20]. These advantages can be used to build isocompliant arterial prostheses (Gershon et al., 1990, 1992), intervertebral disks duplicating the natural structure (Ambrosio et al., 1996) or fixation plates and nails with controlled stiffness (Veerabagu et al., 2003) [20]. Radiolucency is also considered to be another potential advantage for some applications. Radiolucency is also considered to be another potential advantage for some applications [20]. A typical example is the external or internal fracture fixation devices not shielding the bone fracture site from the X-ray radiography [20]. Flexibility, strength and lightweight design have made polymeric composite materials, mainly carbon fiber, the ideal materials for orthotics that can return walking and even athletic performance to impaired people (Dawson 200) [20].

Some of the main reinforcing materials that have been used in biomedical composites are carbon fibers, polymer fibers, ceramics, and glasses. The reinforcements are either inert or absorbable depending on the application [20].

Composite materials can be manufactured using various technologies. The fabrication process used is dependent on the type of filler (particle, short or long fiber) and matrix (thermoplastic or thermosetting) [20]. Some use solvents whose residues could affect the biocompatibility of the material and are therefore not applicable to the manufacture of biomedical composites [20]. The selection of the most suitable manufacturing technology is also influenced by the relatively low production volumes compared with other applications and the relatively low dominance of the manufacturing costs over the overall cost of the device [20]. Common fabrication technologies for composites include: Hand layup, spray up, compression molding, resin transfer molding, injection molding, filament winding and pultrusion [20].

1.3 Summary/ Organization of Thesis

This thesis begins with the outline of relevant background information. The first chapter covers range of topics from biomaterials and total hip joint replacement. They further elaborate hip implants, types of wear, friction and corrosion. The investigation of two alloys in different pH environments is covered in chapters 2 through to 4 which engulfs the characterization methods, the material preparation and methodologies used in completion of this experiment.

The thesis ends with chapter 5 which provides concrete conclusions from the experiments conducted and future work to be done to provide more information and further support results attained.

Chapter 2: Experimental methods and characterizations

2.1 Mechanical properties

Structural stability is the most important for load bearing joint implants. Daily motions of patients lead to a multi-axial cyclic loads including axial, bending and shear load. As a result, the continuous relative motion, known as fretting fatigue takes place at the interlocked modular interface such as femoral head-stem interface. Therefore, strengths, ductility, and wear resistance are very critical characteristics of implant materials. In addition, this complex mode of loads is applied to the implants in the corrosive environment. Consequently, it is necessary to understand modification of strengths and wear resistance in the reactive condition. In this chapter, a brief discussion of mechanical integrity of metallic implant materials.

The mechanical properties such as the young's modulus, hardness, ultimate strength, fracture toughness, modulus of resilience, endurance limit and fatigue strength are imperative in choosing metallic implants. These properties also help in predicting the life of the material being used in manufacturing of the implant. Elastic modulus which is the measurement of an object's resistance to elastic deformation under any type of stress was a key factor in determining parameters such as the normal load to be used [35]. The yield strength is also a property of a material at which it undergoes plastic deformation under stress [36]. Yield strength is typically taken as 0.2 the unstressed length. Ultimate strength of a material can be defined as the ability of the material to endure tensile loads [37]. This property can be characterized by using a tensile stress test, thus the use of example an Aeres mechanical tester to apply a tensile load to the material. Fracture toughness can simply be defined as a materials ability to resist fracture (resistance of a material to brittle fracture) [38]. The modulus of resilience of a material is the maximum energy consumed per unit volume without causing distortion to the material [39]. The endurance limit also sometimes known as the fatigue limit is the range of cycle stress that the material can endure without causing any type of fatigue failure [40]. This can be characterized by using the tension-compression testing (alternating the samples between tensile and compressive loading) and tension-tension testing (exposing the samples to cyclic tensile amplitude), bending and torsion [41]. Some of these properties such as elastic modulus, yield strength and ultimate

strength can be measured using a nanoindentation technique which involves the use of a nano-indenter using a tip harder than that of the metal preferably a Berkovich diamond tip.

Titanium alloys are used for biomedical applications because of its high biocompatibility, corrosion resistance and specific strength unlike other implant materials [42]. There are different types of titanium alloys which are used in the biomedical industry [42]. These are Ti-6Al-7Nb [43] and Ti-5Al-2.5Fe [44] and Ti6Al4V alloys to name a few. Listed in Table 3 are titanium alloys used in biomedical applications. Ti6Al4V is the most commonly used titanium alloy. It is preferred because of its ease of machinability and outstanding mechanical properties. It is not only used in the biomedical field but also in the aerospace, automotive and marine fields as well. This is due to its outstanding performance for weight reduction [44]. The Ti6Al4V alloy which is the main focus in this experiment, is an alpha-beta titanium alloy which has a high strength-weight ratio and high corrosion resistance. CoCrMo alloys however are used for biomedical applications such as implants because of its high wear and corrosion resistance [44]. CoCrMo alloys are comprised of 58.9-69.5% Co, 27.0-30%Cr, 5.0-7.0%Mo, and small amounts of other elements (Mn, Si, Ni, Fe and C), which follows the ASTM standard for cast alloys and wrought alloys (F-75 or F-1537) [45]. These alloys are used in areas where high stiffness or a highly polished and extremely wear-resistant material is required which is why it is sometimes the preferred material of choice for knee implants, MoM hip joints and dental prosthetics [45]. In table 4 below are some CoCrMo alloys used in the biomedical field.

Table 3: Titanium alloys used in biomedical field

Ti6Al4V ELI (Wrought: ASTM F136 and forged: ASTM F620); α+β type	Ti-13Nb-13Zr: near β type (USA), low modulus
Ti-5Al-3Mo-4Zr: α+β type (Japan)	Ti-12Mo-6Zr-2Fe: β type (USA), low modulus
Pure titanium (ASTM F67): Grade 1, 2, 3 and 4	Ti-15Mo: β type (USA), low modulus
Ti6Al4V (Casting: F1108): α+β type	Ti-16Nb-10Hf: β type (USA), low modulus
Ti-5Al-7Nb (ASTM F1295): α+β type (Switzerland)	Ti-15Mo-5Zr-3Al: β type (Japan), low modulus
Ti-5Al-2.5Fe (ISO/DIS 5832-10): β rich α+β type (Germany)	Ti-15Mo-3Nb: β type (USA), low modulus
Ti-15Sn-4Nb-2Ta-0.2Pd: α+β type (Japan)	Ti-35.3Nb-5.1Ta-7.1Zr: β type (USA), low modulus
Ti-15Zr-4Nb-2Ta-0.2Pd: α+β type (Japan)	Ti-29Nb-13Ta-4.6Zr: β type (Japan), low modulus

Table 4: Cobalt based alloys used in biomedical field

Co-28Cr-6Mo cast
Co-28Cr-6Mo wrought 1,2,3
Co-19Cr-17Ni-14Fe-7Mo-1.5Mn
Co-35 Ni-20Cr-10 Mo
Co-20Cr-15W-10Ni-1.5Mn

2.2 Corrosion resistance

2.2.1 OCP

Corrosion usually happens at a rate determined by an equilibrium between opposing electrochemical reactions. The initial reaction is an anodic reaction. This occurs when a metal is oxidized causing the release of electrons into the metal [46]. The alternative is a cathodic reaction. In this type of reaction, a solution species (often O_2 or H^+) is reduced, removing electrons from the metal. Often when these two reactions are in equilibrium, electron flow from

each reaction is balanced and no net electron flow occurs. Both reactions can occur on one metal or on two different metals that are electrically connected [46].

The method by which the anodic and cathodic reactions are kept in balance is referred to as the potential of the metal. The electrochemical potential of a metal is dependent on the half reaction produced by the current [46]. For example, when the anodic reaction releases too many electrons into the metal, the excess electrons released shift the potential of the metal more negative, which ends up slowing the anodic reaction and increasing the cathodic reaction. This counteracts the initial perturbation of the system [46].

To record the open circuit measurement, a potentiostat with a three-electrode unit was used. The potentiostat is used to measure the ion concentration in an electrolyte by virtue of the current and voltage measurements. As mentioned earlier, a three-electrode unit was used for open circuit measurement. These three electrodes are the working electrode, counter electrode and reference electrode. The working electrode is the polished alloy embedded in epoxy be it Ti6Al4V or CoCrMo, the counter electrode is a platinum wire and the reference electrode is a saturated calomel electrode which is known for its accuracy in electrochemical measurements. Everything is put together with a customized stage as part of a final configuration before fretting corrosion is began. Using the principle of the Hertzian contact theory between a sphere and an elastic surface, an alumina sphere with a 3mm diameter is used to induce scratching on the surface of the alloys which is submerged in an electrolyte. Changes in potential in the OCP shows changes in the surface layer of the alloy. It could be a re-passivation process thus formation of oxide layer on the surface of the metal or a de-passivation process thus the breakdown of oxide layer on the surface of the metal.

2.2.2 Potentio-static/dynamic polarization

The need to understand electrochemical techniques are optimal for the study of the corrosion process because corrosion occurs through electrochemical reactions [46]. An electrochemical study can be done using a potentiostat. The potentiostat allows for the controlled change of a potential of a metal and measure the current that flows as a function of potential. A potentiostatic polarization is the measure of current across the surface of the metal over a period of time. Polarizing a sample means forcing the potential of the metal surface in a solution away

from an open circuit potential. The current (response) of the sample is measured as it is polarized. This response is used to develop a model of the sample's corrosion behavior [46].

A potentiostatic polarization test is another way of measuring the electrochemical corrosion of a metal surface. In a potentiostatic polarization test, a uniform voltage is run across the surface of the metal to obtain the change in corrosion current (I_{corr}) over a period of time. As aforementioned, the corrosion rate and current are dependent on factors such as the type of metal, solution movement and many others. In order to ensure electrochemical corrosion is occurring while running a potentiostatic test, a linear sweep voltammetry is run to obtain the potential at which oxidation of iron occurs on the surface of the metal. It varies for different metals but in CoCrMo, the maximum current should not exceed 1.5V. An electrochemical series chart can be used to obtain the range of potentials at which deionization of present chemicals in an alloy occurs. This helps with giving an idea of what the maximum current could be before running the linear sweep voltammetry. Individual oxidation of the various elements will occur at the given potentials if the chemical composition of the alloy is not uniform. For a uniform chemical composition alloy, oxidation would still occur but the individual elements will not stand out.

Table 5: Electrochemical Series Table for various common elements in CoCr alloy

Reaction	Potential (Volts)
$H_2MoO_4 + 6H^+ + 6e^- \rightarrow Mo\ 4H_2O$	0.00
$Co^{+2} + 2e^- \rightarrow Co$	-0.28
$Fe^{+2} + 2e^- \rightarrow Fe$	-0.4402
$Cr^{+2} + 2e \rightarrow Cr$	-0.557

Table 6: Electrochemical series table for various common elements in Ti6Al4V alloy

Reaction	Potential Range (Volts)
Titanium	0.04 to -0.12
Aluminum	-0.76 to -0.99
Vanadium	-0.26

From the list presented above, the maximum potential required to initiate oxidation of iron in the alloy is 0.00 volts so the 1.5 volts is well above the oxidation potential.

2.3 Friction and wear resistance

2.3.1 Friction

Friction is a force which opposes relative motion between contacting systems [8]. Its nature is complicated hence making it a little difficult to comprehend but it can be characterized using a variety of mechanical testing techniques. A fundamental characteristic of frictional force is that it is parallel to surfaces between the interacting surfaces [8]. Force of friction is known to have two main types i.e. kinetic and static frictions. In a system experiencing kinetic friction, it is observed that the systems in contact move relative to each other with a significant displacement. In a case of static friction, there is no relative motions between the systems in contact [47]. Simply put, there is no motion between objects, the magnitude of the static friction is $f_s \leq \mu_s N$ and that of the kinetic friction is is $f_k = \mu_k N$. Even in the perfect smooth surface contact, friction is as a result of the roughness of the attractive forces between molecules making up the objects or surfaces in electrical or chemical bonding [47]. In this experiment, wear is also characterized using frictional force. Frictional force is measured using frictional table installed with the nano-indenter. The friction table measures the frictional force, normal force and CoF of friction on a microscale.

2.3.2 Wear: abrasion, adhesion, contact fatigue

The damaging, deformation and gradual removal of material at solid surfaces is known as wear. It can be mechanical or chemical [48] and the study of this phenomenon and its processes is known as tribology [48]. In machine elements, wear in conjunction with fatigue and creep, cause functional surfaces to degrade, subsequently leading to loss of functionality or failure [49]. Wear ultimately yields in generation of debris of different sizes, shapes and chemical compositions [50]. Particle properties depend on load applied, sliding speed, environment and other parameters [51]. Wear particles can vary according to shape. They include plate-shaped particles with aspect rations of 2-10, which occur as a result of accumulated plastic deformation, and ribbon-shaped particles with aspect ratios higher than 10 also caused by abrasion [51].

These particles induce mechanical damage, however, sometimes the aftermath become more relevant. For instance, in artificial joint replacements, wear debris triggers the autoimmune reaction and leads to a failure of the joint over time [52]. The severity of the reaction is known to be dependent on the wear particles number, shape, size and surface area [53]. The rate of wear is also dependent on type of loading, motion, temperature and lubrication. There are different types of wear mechanisms. Namely, adhesive wear, abrasive wear, surface or contact fatigue, fretting wear, erosive wear and corrosion wear.

According to ASTM international, wear due to abrasion is defined as material loss due to hard protuberances that are forced against and moved along a solid surface [54]. It is identified according to the type of contact and the contact environment [55]. The mode of abrasive wear is can be determined by the type of contact. The two main modes are two-body (occurs when the grits or hard particles remove material from the opposite surface) and three-body (occurs when particles are not constrained and are free to roll and slide down a surface) abrasive wear [48]. The common terms or ideas used to describe a two-body abrasion mode
is comparable to a material being removed or displaced by a cutting or plowing operation [48]. In that of the three-body abrasion mode, the contact environment determines whether the wear is qualified as open or closed [48]. When surfaces are sufficiently displaced independent of one another it is known as an open contact environment. The manner of material removal is influenced by certain factors such as plowing, cutting and fragmentation [48]. Plowing usually happens when debris is displaced to the side, away from the wear particles, which ultimately

results in the formation of grooves that do not involve direct material removal [49]. Cutting however, occurs when there is separation of material from the surfaces primarily as debris or microchips with little or no material displaced to the sides of the grooves. It is comparable to conventional machining [49]. Fragmentation also occurs when there is separation of material from the surface through a cutting process and the indenting abrasives causes localized fracture of the wear of the material. Propagation of these cracks freely occur around the wear grooves which results in additional removal of material by spalling [49].

Adhesive wear is a type of wear found between surfaces undergoing frictional contact and generally defined as the unwanted displacement and attachment of wear debris and material compounds from one surface to another [48]. Adhesive wear can be put into two main categories: adhesive wear caused by relative motion and plastic deformation which create wear debris and transfer of material from one surface to another and cohesive adhesive forces which holds two surfaces together though they are separated by a measurable distance with or without any actual transfer of material. Adhesive wear in general occurs when two bodies slide over or are pressed into each other, which induces material transfer. This is sometimes described as plastic deformation of very small or minute fragments within the surface layers [48]. The surface roughness or asperities found on each surface affects the severity of how oxide fragments are pulled off and added to the other surface, this is partly due to the strong adhesive forces between atoms but also due to the build-up of energy in the plastic zone between the asperities during relative motion [56]. The surface attraction varies between different materials but are heightened by a rise in the density of the surface energy. To a certain extent, most solids will adhere on contact however, certain natural phenomenon such as oxidation films, lubricants and contaminants generally suppress adhesion and spontaneous exothermic reactions between surfaces generally create a substance with low energy status in the absorbed species [57]. Adhesive wear leads to an increase in roughness and production of protrusions above the original surface [57].

Contact fatigue, which is commonly found in ball or roller bearings, is a surface-pitting type failure. There are found in metal alloys, ceramics and cements. It results from a contact or Hertzian stress state which is its main difference from classic structural fatigue [57]. This localized stress state results when curved surfaces are in contact under a normal load. Usually,

there is motion of one surface over the other in a rolling motion. The contact geometry and the motion of the rolling elements produces a different subsurface shear stress [57]. Plastic strain builds up on the subsurface with increasing cycles until there is generation of a crack. The crack subsequently propagates until a pit is formed [57]. Initiation of pitting causes the bearing or ball to become noisy and rough running. If this is allowed to continue, fracture of the rolling element and failure occurs. Fractured races are caused by fatigue spalling and high hoop stresses [57]. Rolling contact components usually have a fatigue life thus the number of cycles to develop a noticeable fatigue spall unlike structural fatigue which has no endurance limit [57].

2.3.3 Standard test methodologies

In this experiment, a scratch test using the ideology of reciprocating wear was performed on two metallic surfaces. Namely, Ti6Al4V and CoCrMo to imitate cyclic contact fatigue during articulations in a total joint replacement (hip prosthesis) during daily motions. In order to achieve this, a Nanovea nanoindenter was used for the fretting fatigue contact experiment. This tester has a micro newton scale load cell and a depth sensor with a nanometer scale and a high-resolution step-motor motion stage. The load cell is used to monitor exact normal loads while the piezoelectric feedback module is used to measure the displacement responses. The motion stage also controls the lateral motion of the sample relative to its vertical spherical slider motions. A 3mm spherical Aluminum silica ceramic was used to perform reciprocating scratch. This 3mm sphere was glued to a customized non-conducting slider material. The wear test was conducted in three different environments. A phosphate buffer solution with a pH of 7.4, a sodium lactate solution with a pH of 4 and 2 to simulate a corrosive body fluid environment.

Hertzian contact stress between a sphere (alumina sphere) and an elastic half space (CoCrMo and Ti6Al-4V) was invoked to evaluate the elastic normal loads as presented in the figure below.

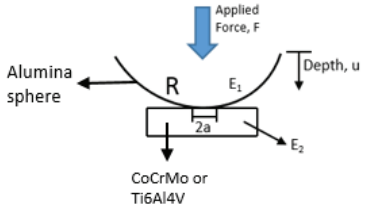

Figure 3: Hertzian contact between a sphere and an elastic half-space. R-radius of alumina sphere, E_1- elastic modulus of alumina sphere, E_2- elastic moduli of associated body, u-depth, a-contact area.

From the figure above, R will be the radius of the alumina sphere, E_1 the modulus of elasticity of the alumina sphere and E_2 the modulus of elasticity of CoCrMo or Ti6Al4V and u the depth. The depth of indentation u is given as:

$$u \cong \left(\frac{2F^2}{E_*^2 R}\right)^{1/3} \text{.....Equation 1}$$

$$\frac{1}{E_*} = \frac{1}{2}\left(\frac{1-v_1^2}{E_1} + \frac{1-v_2^2}{E_2}\right) \text{.....Equation 2}$$

E_1 and E_2 are the elastic moduli and v_1 and v_2 the Poisson's ratios associated with each body. The reciprocating wear test parameters were selected according to the normal walking motion which is an oscillating frequency of 1 Hertz. As aforementioned, fretting fatigue test was done for 1800 cycles which is equivalent to 60 minutes. The slider speed of 12 millimeters per minute was applied to a scratch length of 200 µm. Presented in table 7 below is a summarized test parameters for the experiment.

Table 7: Wear Test Parameters

Method	Parameters
Type	Reciprocating
Load (mN)	Constant (143)
Scratch Length (µm)	200
Scratch Speed (mm/min)	12
Specimens	CoCrMoTi6Al4V
Environment	PBS, Sodium Lactate

An optical microscope was used to investigate the size and shape of wear trenches. This will inherently help examine the mechanisms of wear and corrosion of any debris developed. The force of friction is measured with the aid of a pre-installed friction table which converts the frictional force to the coefficient of friction during fretting contact tests. The result will also aid in the comprehension of surface damage on the two surfaces.

The need to understand electrochemical techniques are optimal for the study of the corrosion process because corrosion occurs through electrochemical reactions [26]. An electrochemical study can be done using a potentiostat. The potentiostat allows for the controlled change of a potential of a metal and measure the current that flows as a function of potential.

The open circuit measurement was measured using this said potentiostat which uses a three electrode method to measure the ion concentration in a liquid environment. The polished and cleaned samples acted as the working electrode, while a saturated calomel electrode (SCE) was the reference electrode and a titanium wire was the counter electrode. These electrodes along with the samples embedded in epoxy were placed in a customized stage to measure fretting contact while exposed to the electrolyte solution or environment. The arrangement which includes a 3mm alumina-silica ceramic sphere moving against stationary titanium or cobalt sample to apply large contact stresses under low loads. The configuration was done such that only the spherical alumina-silica and exposed metal surface of the sample were totally immersed in the electrolyte. The metal was kept in the solution for 60 minutes before any scratch was performed. This was done to allow stabilization of the electrolyte. The fretting contact

configuration was connected to the potentiostat to measure the ion concentration in the electrolyte. Initially the open circuit potential was run to ensure corrosion was at equilibrium. Changes in OCP is measured as a function of time to analyze the performance of both alloys in different environments/ electrolytes under a constant fretting contact condition. The corrosion test were repeated at least twice to verify reproducibility of the test results. The type of reaction whether anodic or cathodic can be determined from the change in OCP measurements which occurs on the surface of the metal specimen depending on the passive surface layer.

Repassivation of the oxide layer on the metal surface increases the potential over time meaning an anodic reaction is occurring versus the reference electrode. Likewise a decrease in potential is caused by depassivation of the oxide layer on the metal surface. Electrochemistry of corrosion is dependent on factors such as load being applied, surface area, chemical composition of the electrolyte, frictional force and many more.

The absence of an oxide layer can cause the dissolution of metals in a liquid substrate. Alloys such as Ti6Al4V and CoCrMo possess some amount of oxide layer which almost makes them immune to dissolving in a liquid substrate but application of a voltage to the liquid substrate can cause passivation or depassivation of this said oxide layer. This imperative in the comprehension of corrosion process in metals. The ability of a metal to resist corrosion is known as polarization resistance. This is usually dependent on the presence of oxide layer on the metal substrate. Potentiostatic Polarization test is performed to investigate corrosion behavior at constant voltage when fretting is initiated. Different voltages are applied across the surface of the metal to measure the current density over time.

Chapter 3: Materials and Preparations

3.1 CoCrMo and Ti6Al4V

Both of the metal alloys were manufactured using the Electrical Discharge Machining (EDM) method to a 1.00mm x 2.54mm x 22.95mm dimensioning. The EDM method is preferred in industry because it can be used to cut metals to precise dimensions without altering its chemical and physical properties all the while minimizing residual stress. These samples were then embedded in epoxy to easily polish the surface.

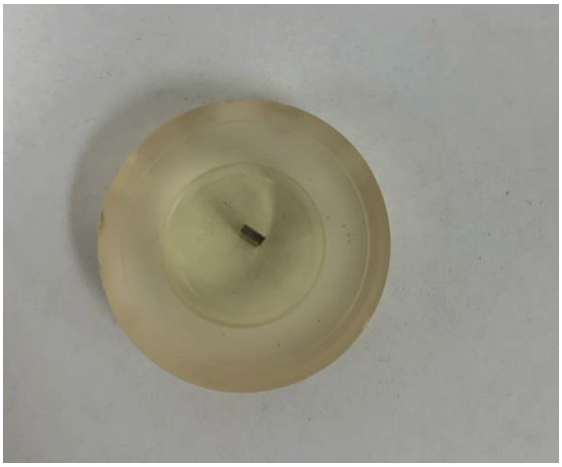

Figure 4: Embedded 1mm x 2.54 mm x 22.95mm sample in epoxy 10 (resin):3 (hardener)

3.2 Sample preparation

The metals were embedded in epoxy with a resin hardener combination of 10:3 (10 parts resin, 3 parts hardener) and left to dry for 24 hours after which they were grinded and polished using 600 grit, 1200 grit and 2400 grit size Silicon Carbide paper and finally a 0.05 μm colloidal silica and alumina on an ultrapad polishing cloth and a chemomet polishing cloth respectively for about 10-15 minutes until it had a mirror finish and then rinsed. Before performing any experiment, all samples were sonicated in acetone, methanol and de-ionized water for 180 seconds (3 minutes). A non-conductive ceramic tip is used to induce fretting on the exposed surface of the specimen in the electrolyte so as to observe the electrochemical responses. This non-conductive ceramic tip is made of a 303 stainless-steel rod (1.59 mm diameter) cut to a

desired and encased in a ceramic tubing with a 3mm diameter alumina silica sphere attached to one end of the non-conductive tip. The tip is then sonicated for 180 seconds in de-ionized water.

Figure 5: Struers Pedmax-2 Polisher used to polish samples

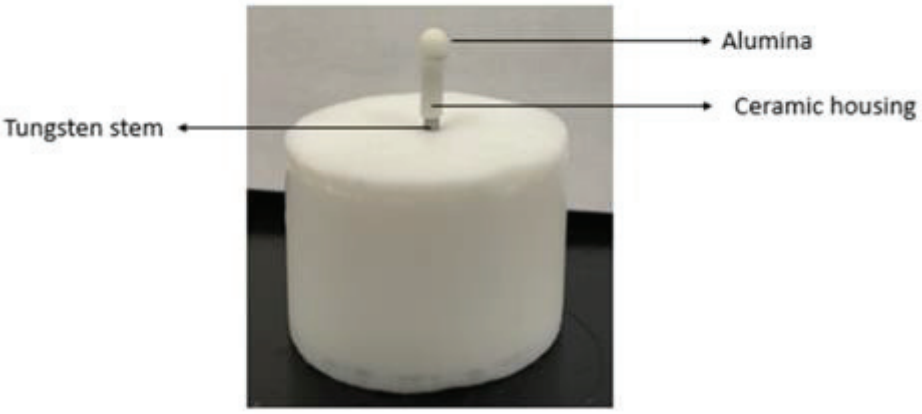

Figure 6: Indenter tip

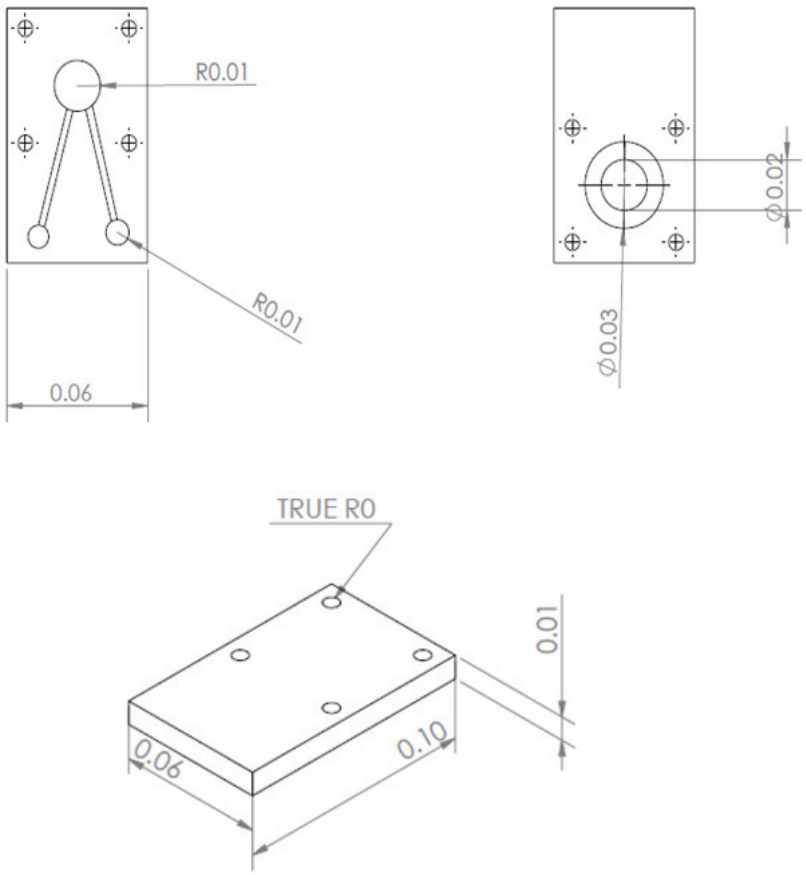

Figure 7: Orthographic drawing of tribochemical cell. All dimensions are in inches

A custom tribochemical cell was designed to conduct the electrochemical tests. This cell came in 3 parts, a bottom plate made of steel to provide stability to the cell, another bottom part made of nylon which ensures that the metal alloy surface (working electrode) is in contact with an aluminum foil via a silver paste to electrically connect to the potentiostat while also preventing any leakage of the electrolyte. The top part also made from Nylon has three holes and a groove. The larger hole which is for the sample embedded in epoxy, has an O-ring fitted to it to prevent the electrolyte from flowing out and subsequently increasing the surface area being investigated. The two small holes are for the counter electrode which is a platinum wire and the Gamry Saturated Calomel Electrode (SCE)/ reference electrode. The groove was to allow the flow of fluid to these holes to enable measurement of potential across the surface of the metal. The electrolytes which are PBS (7.4 pH) and Sodium lactate solution (pH 4 and 2) were made by

diluting a 0.1m of hydrochloric acid with 1 gram of sodium lactate powder. The electrochemical apparatus was installed on the friction table to monitor friction forces during fretting and mounted on the nano tester machine to perform a mechanical-chemical test.

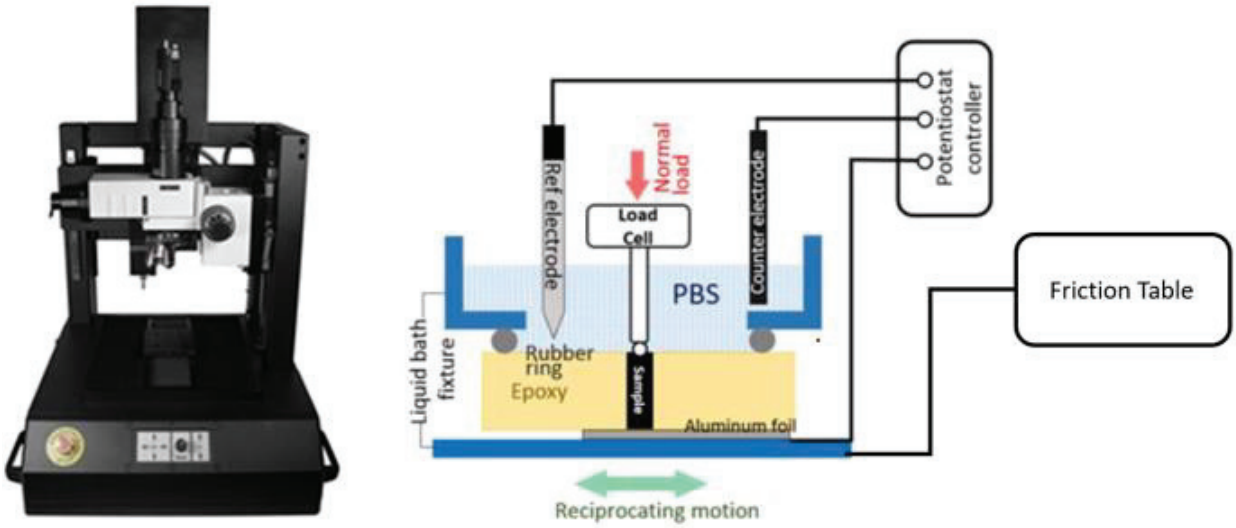

Figure 8: NANOVEA scratch tester with the final set-up before fretting commences

3.3 Preliminary measurements: roughness (R_a and R_q), hardness, elastic modulus, yield strength

Some preliminary measurements were recorded before electrochemical tests were started. This includes the roughness (Ra and Rq), hardness, elastic modulus and yield strength of both Ti6Al4V and CoCrMo samples. The roughness of the surface of the metal alloys was obtained by performing a linear scan (1mm length and 250µm step size) using the3D Non-Contact Optical Profiler Module. The obtained values were run through a MATLAB code to provide the final values for the roughness which came out to be 0.04. The hardness, elastic modulus and yield strengths were obtained using the NANOVEA hardness tester. The samples were indented using a Berkovich diamond tip at a load of 200mN. Below are values for the respective metal alloys

Table 8: Elastic Modulus and Hardness of Ti6Al4V sample

Elastic Modulus (Gpa)	Hardness (Gpa)
134	5.07

Table 9: Elastic Modulus and Hardness of CoCrMo sample

Elastic Modulus (Gpa)	Hardness (Gpa)
299.3	5.96

As seen in tables 8 and 9 above, the Cobalt Chromate alloy is superior in mechanical properties than the Titanium alloy.

Chapter 4: Results and discussion

Electrochemical tests during fretting include open circuit potential results and current density with applied potential measured during cyclic sliding contacts on both CoCrMo and Ti6Al4V surfaces. The results were repeated in different physiological environments. PBS solution represents normal healthy body fluid, and sodium lactate solutions with two different pH levels represent unhealthy inflammatory environments. The deteriorated passive film by sliding contact causes a significant potential drop to the negative followed by a subsequent increase in anodic current. [49]. The measured coefficients of friction are correlated to the electrochemical changes including OCP and fretting current density during active mechanical stimuli. This observations will illustrate the effect of the physiological environments on the mechanical wear and corrosion damage. Therefore, evolution of the potential and current during continuous sliding would explain the metal oxidation chemistry of the alloys against wear and corrosion.

4.1 Fretting Corrosion Test in PBS Electrolyte (pH 7.4):

The potential change by reciprocating motion with a constant normal load of 143mN was monitored before fretting (dwell), during fretting (active articulations) and after fretting motion (recovery) on CoCrMo and Ti-6A-4V. As shown in Figures 9-11, the potential was allowed to stabilize for an hour, and then the reciprocating motion using the spherical alumina was applied at 143mN. There was a significant potential drop on both CoCrMo and Ti6Al4V surfaces due to the exposure of metal via a damaged oxide layer to a PBS solution. However, the potential rapidly increased instantaneously and gradually increased during continuous fretting motions (Figure 9), while the potential of CoCrMo continually decreased until the fretting is ceased (Figure 10). From the average potential drop by fretting contact compared in Figure 11, it is evident that the potential of Ti6Al4V drops as soon as the slider motion is initiated but spontaneous repassivation occurs and the potential is gradually recovered to its original potential at the dwell period while the fretting motion of the slider is continued. It is notable that the presence of the electrolyte is beneficial to titanium to reform its stable oxide layer. However, during fretting wear on CoCrMo the potential continuously drops until sliding motion is ceased. This shows that the mechanical strength of the reformed chromium oxide layer may not be comparable to the original passive layer formed in ambient. During fretting on CoCrMo surface's rapid fluctuation in potential shows repetition of deterioration-reformation of the oxide layer in PBS[49]. A small potential drop of Ti6Al4V in PBS

describes the effect the electrolyte has on the ion oxidation to activate electrochemical reaction in the alloy. After fretting stops, CoCrMo surface is rapidly re-passivated while Ti6Al4V was readily re-passivated during fretting motion. Therefore, the Ti6Al4V presented desirable oxide chemistry that recovers the damaged surface in the PBS electrolyte.

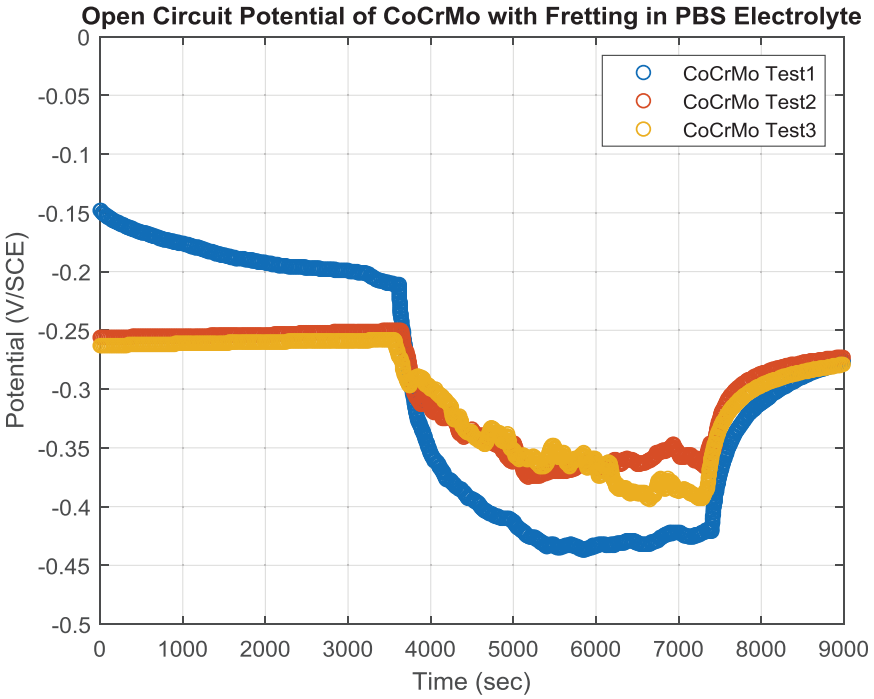

Figure 9: Graph of time vs potential of CoCrMo before fretting, during and after in PBS solution

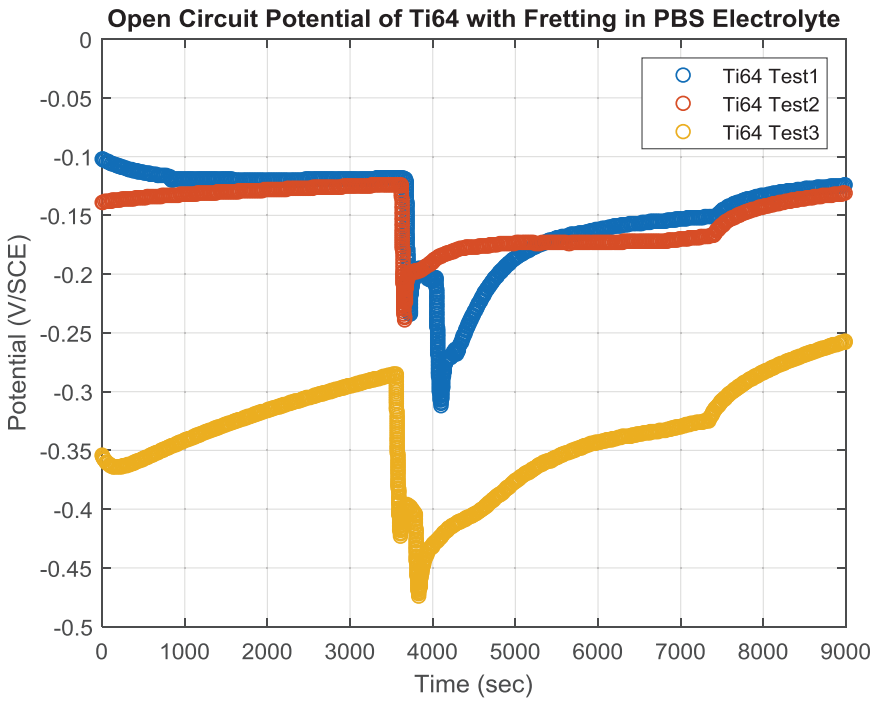

Figure 10: Graph of time vs potential of Ti6Al4V before fretting, during and after in PBS solution

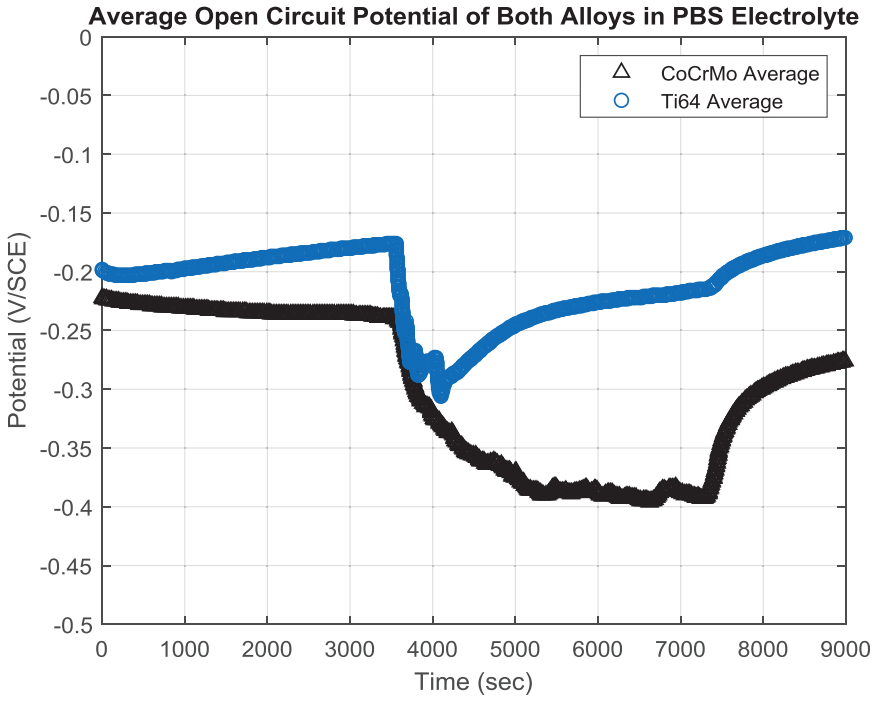

Figure 11: Average OCP on Ti6Al4V ELI and CoCrMo in PBS Solution

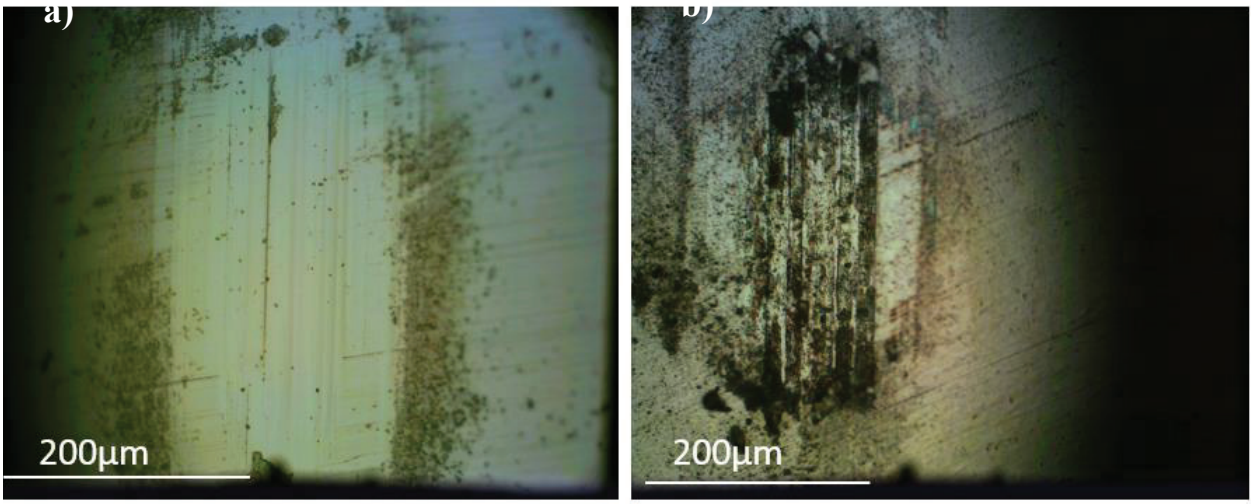

Figure 12: Optical microscope image of alloys in PBS (a) CoCrMo and (b) Ti6Al4V

Figure 12 illustrates wear mechanism of fretting corrosion in PBS captured using the optical microscope. It shows that at the area of contact, the alumina sphere creates grooves parallel to the sliding direction with pits of different sizes visible in between these grooves. In Ti6Al4V dark grey colored regions represent deep wear tracks producing larger wear debris. These oxide flakes are plastically deformed and crushed between interacting surfaces during mechanical action and are agglomerated into fretting tracks. The region on CoCrMo represents the nano-sized corrosion debris mostly made from abrasion of oxide layer that are continuously formed on CoCrMo surface while scratching and removed from its place. CoCrMo undergoes less plastic deformation and fretting marks are clearly visible. The pits on both surfaces are smaller and scratch is not as deep. For Ti6Al4V the wear track is produced by larger wear particles and the overall wear track width is smaller in size due to the three-body wear and subsurface delamination. The scratched area also undergoes extensive damage due to shear deformation and plowing of the ball. The surrounding of the scratched area where debris particulate is smooth.

The potential changes at the onset of fretting and during are summarized in Figures 13-14. In the figure, the negative change describes degradation of the oxide layer thereby accelerating the anodic reaction (dissolution). As mentioned earlier potential drops are observed on the onset of

fretting in CoCrMo followed by a drastic potential drop upon the fretting. The gradual change in potential during successive fretting with low potential drop at the onset of fretting leads to continuous potential changes on CoCrMo surface. For Ti6Al4V surface the positive change of the potential shows that it is responsive to re-passivation, which produces a strong oxide layer that can withstand the frictional forces during fretting. Therefore, the tribocorrosion behaviors of Ti6Al4V in PBS is clearly superior to CoCrMo surface.

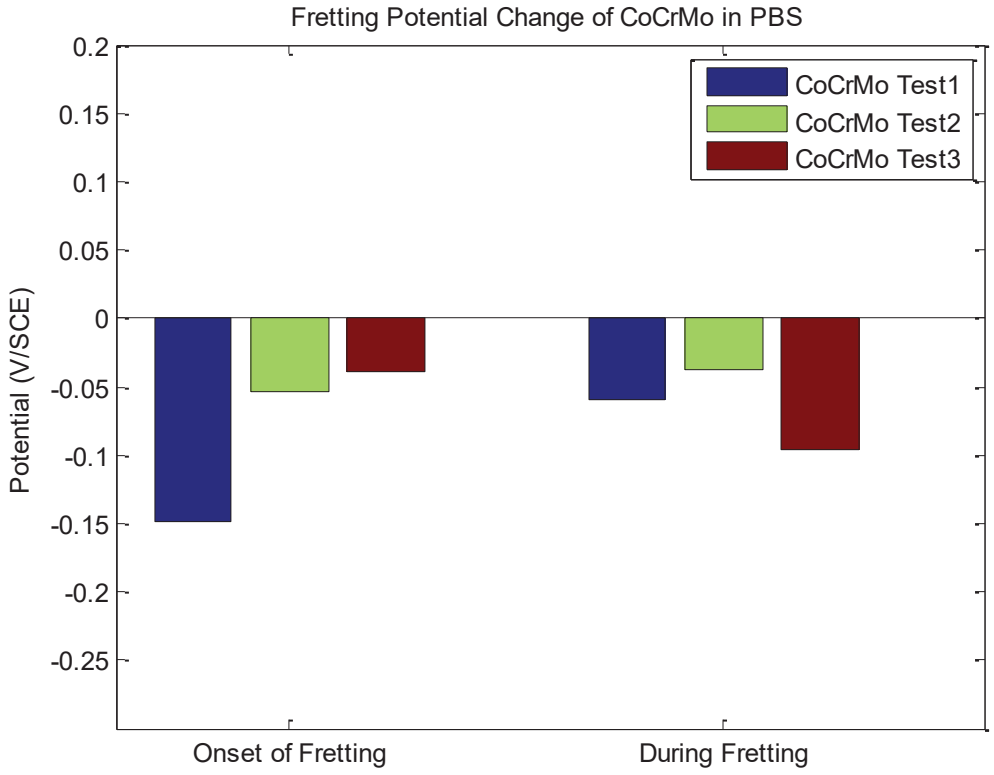

Figure 13: Statistical Analysis of OCP of CoCrMo in PBS (pH7.4)

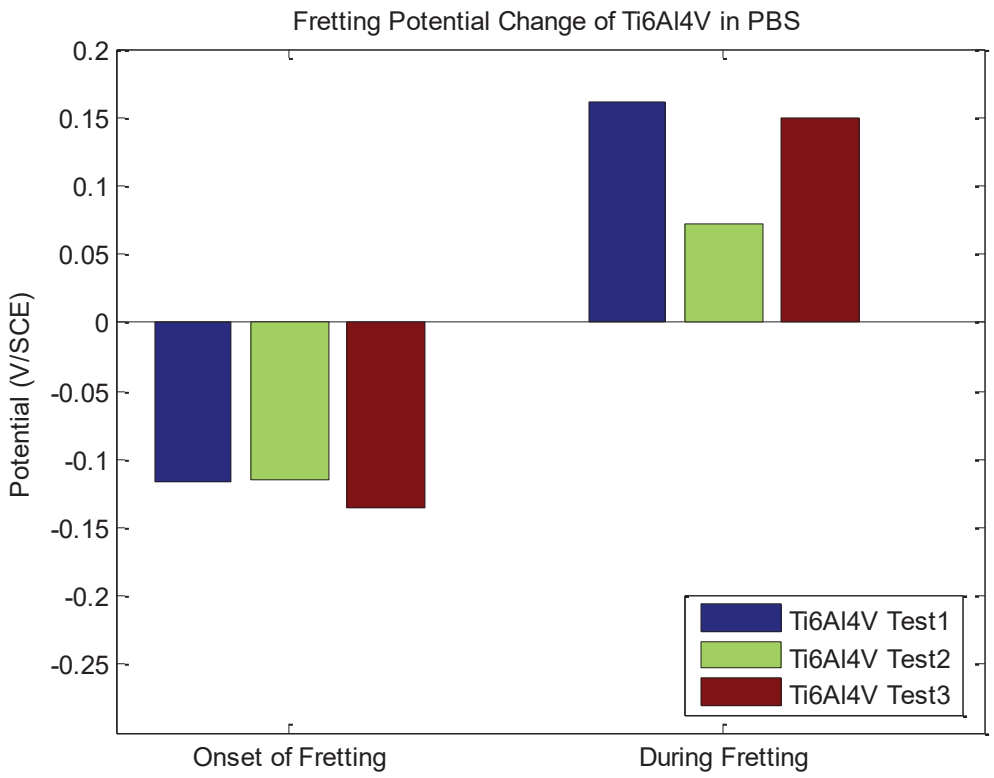

Figure 14: Statistical Analysis of OCP of Ti6Al4V in PBS (pH7.4)

Changes in the coefficients of friction (CoF) measured during fretting experiment in PBS is shown in Figures 15-20. Figures show the ratio between frictional force (tangential force) and normal loads during bilateral movement during forward and backward motions of the spherical tip. The slider motion was controlled at the same speed and distance during the OCP measurements up to 1800 cycles. CoF is closely related to the physical and chemical characteristic of the surface as well as the morphology of the surface including roughness and grain sizes at the small-scale contact.

Two different behaviors are observed on CoCrMo surfaces during fretting in PBS, i.e. during the early stages of sliding, CoF values increased instantaneously up to 50 mm of accumulated sliding distance and gradually increased to 0.8. However, when CoF values began with greater than 0.8, CoF gradually decreases and reached to 0.8 at 50 mm reciprocating distance. At the initial stage of contact up to 15 mm of cumulative scratch distance, the CoF

values are around 0.6 and then rise up to 0.67 of COF and maintain steadily. If the COF values on CoCrMo is as low as 0.5, then COF values gradually increases until it reaches 0.8 on both forward and backward motions. The COF value is stable at an almost constant value throughout the rest of the test. In both cases, friction behavior tends to settle to a stable friction process on CoCrMo.

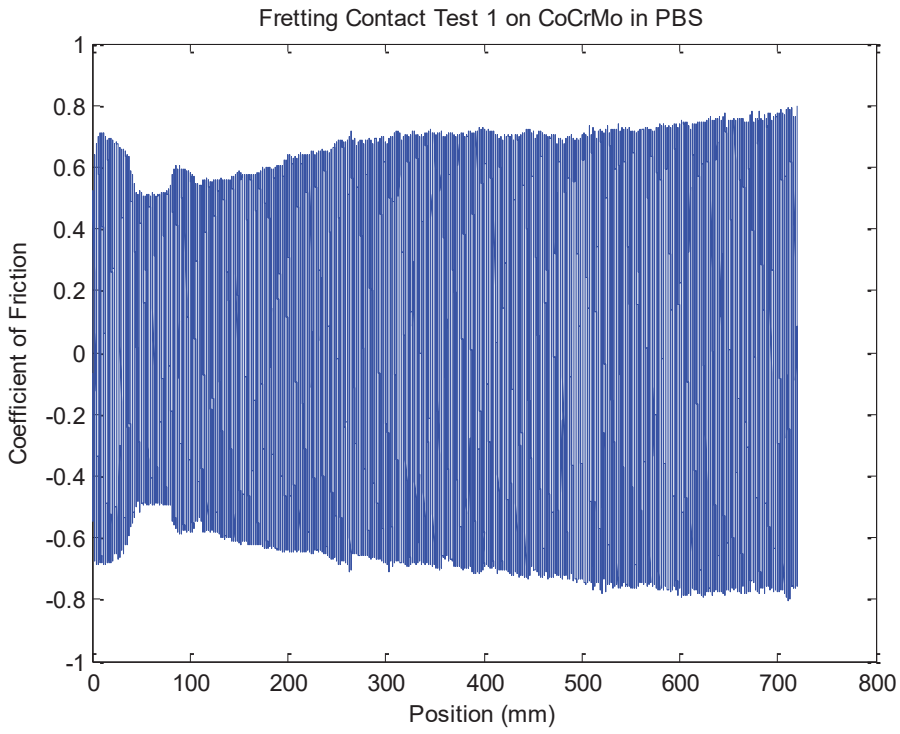

Figure 15: CoF plot of CoCrMo measurement in PBS Test 1

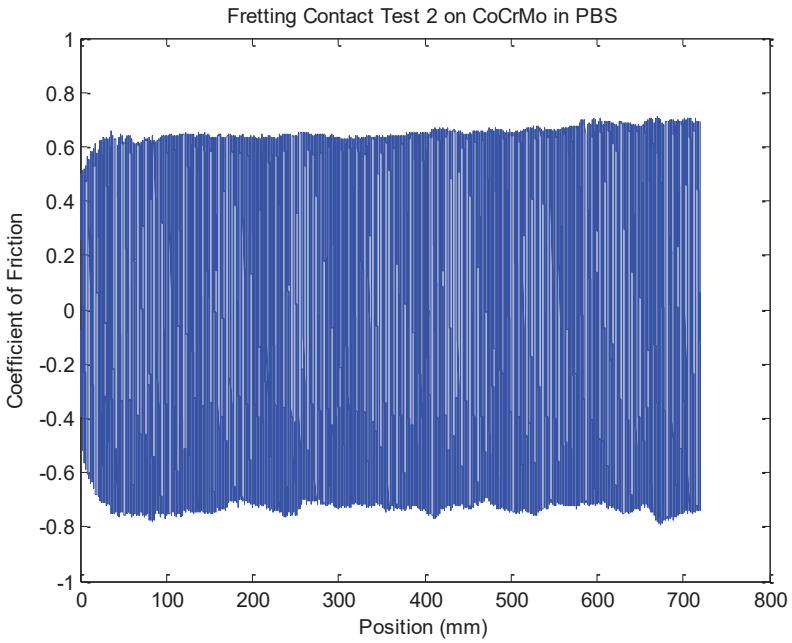

Figure 16: CoF plot of CoCrMo measurement in PBS Test 2

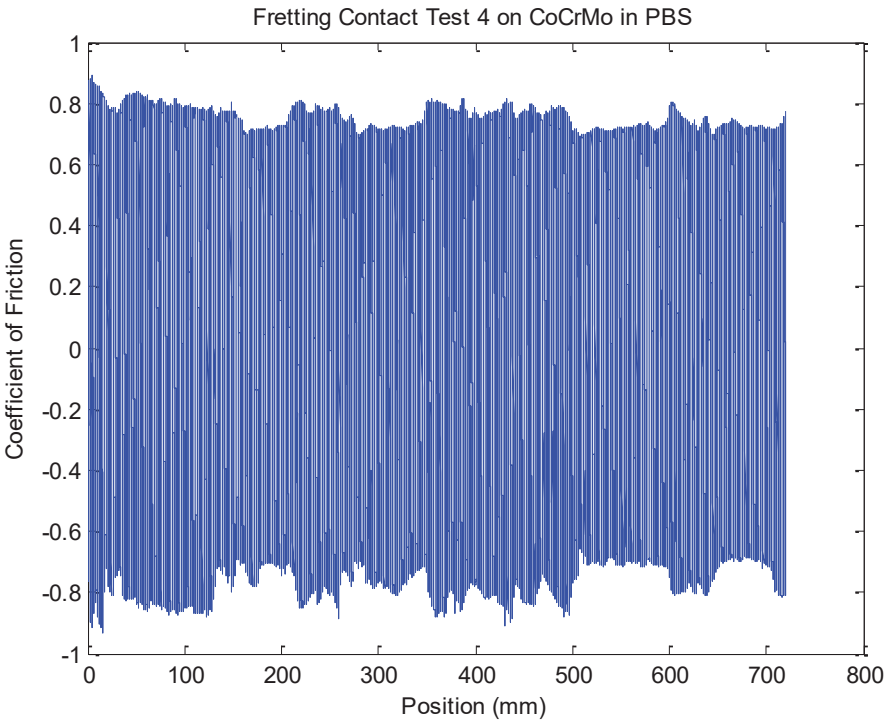

Figure 17: CoF plot of CoCrMo measurement in PBS Test 3

CoF changes on Ti6Al4V surface began with less values of about 0.3 increased to a range of 0.5 to 0.6. Ti6Al4V illustrated more stable mechanical response by maintaining the value throughout the test. Similar to the results from CoCrMo, the friction process at the high cycles presents steady responses. The minor increase in COF for both surfaces suggests locally damaged oxide layer may increase adhesive friction. From the micrographic analysis in Figure 12, the effect of wear debris on COF evolution is not significant.

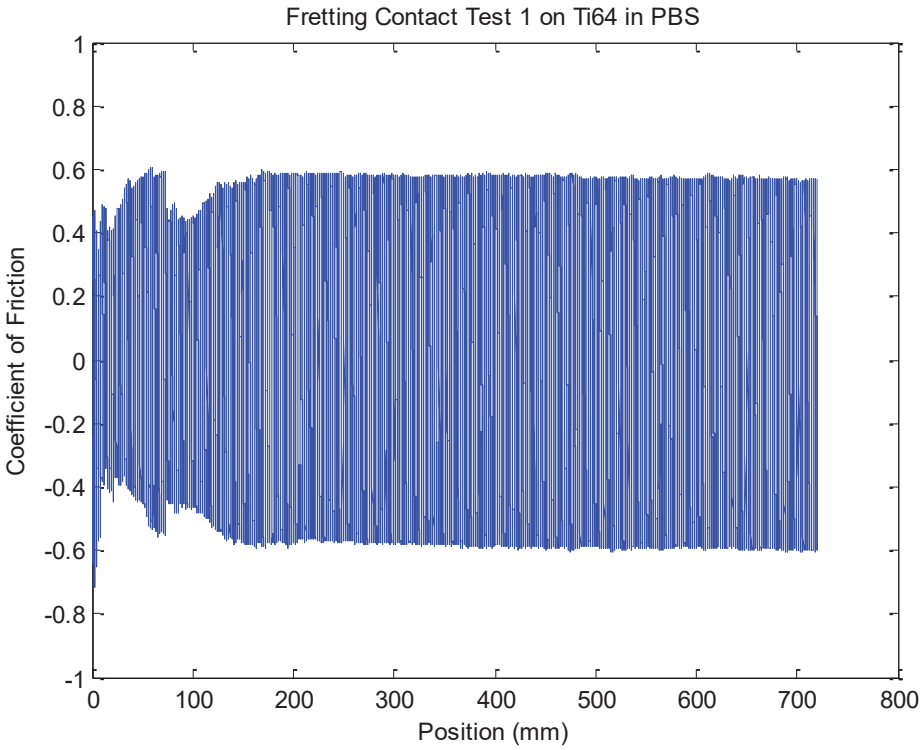

Figure 18: CoF plot of Ti6Al4V measurement in PBS Test 1

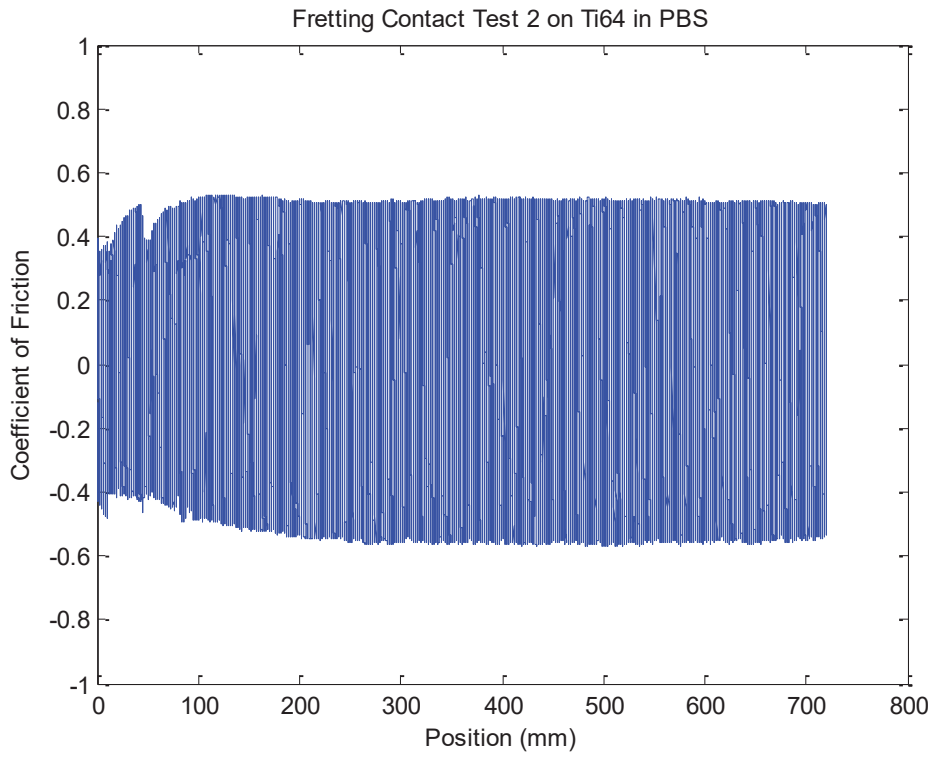

Figure 19: CoF plot of Ti6Al4V measurement in PBS Test 2

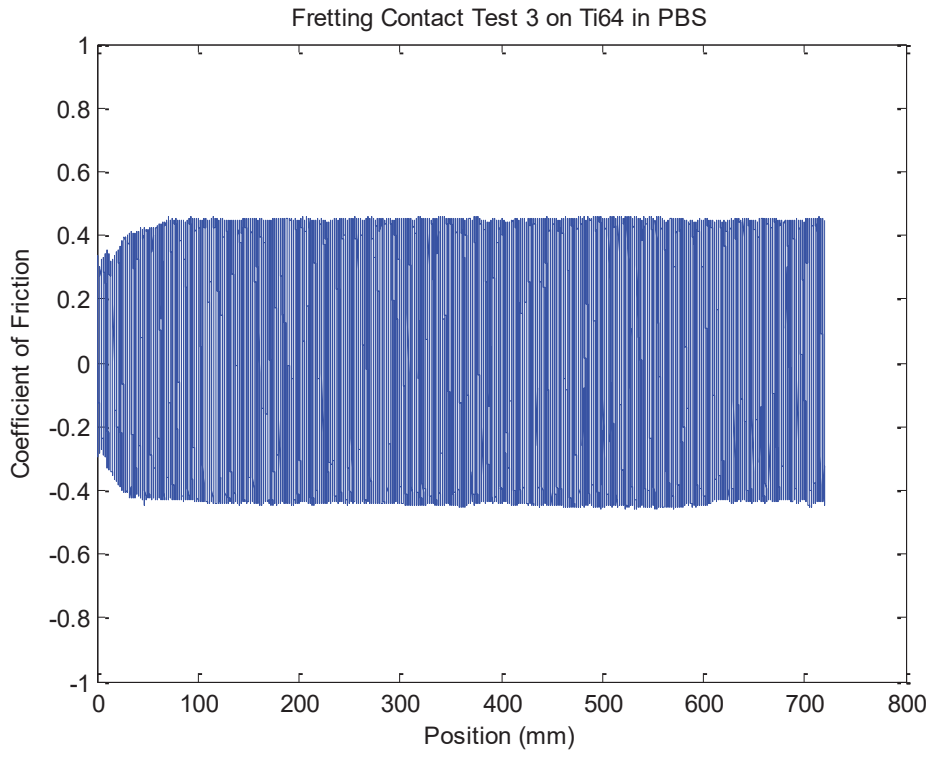

Figure 20: CoF plot of Ti6Al4V measurement in PBS Test 3

Table 10 summarizes the range of CoF values in PBS on both surfaces. Average COF values for both metals in PBS are higher compared to COF values from lower acidic levels at Lactate pH2 and pH4.

Table 10: Maximum and Minimum CoF values in PBS

Material	CoCrMo			Ti6Al4V		
	Test 1	Test 2	Test 3	Test 1	Test 2	Test 3
Forward CoF	0.77	0.66	0.89	0.59	0.53	0.53
Backward CoF	-0.79	-0.85	-0.91	-0.56	-0.57	-0.57

4.2 Fretting Corrosion Test in Sodium Lactate pH 4 Solution:

The potential change by reciprocating motion with a constant normal load was monitored during fretting on CoCrMo and Ti-6A-4V in a sodium lactate solution. The pH level of the lactate solution was adjusted by adding sodium chloride to obtain controlled acidic environment of pH 4.0. As shown in Figures 21-23, overall fretting corrosion processes in sodium lactate pH 4 presented similar behaviors in PBS pH 7.4. There was a significant potential drop on CoCrMo and a minor drop on Ti6Al4V surfaces due to the exposure of metal via a damaged oxide layer to a sodium lactate pH4 solution. During fretting wear on CoCrMo the potential continuously drops until sliding motion is ceased. The potential drop of CoCrMo surface was accelerated up to 5000 seconds (approximately 1000 cycles) and decelerated in the rest of fretting (Figure 21). However, the potential of Ti6Al4V surface instantaneously decreased and maintain the potential values throughout the fretting (Figure 22). From the average potential drop by fretting contact compared in Figure 23, it is evident that the potential of Ti6Al4V slightly drops as soon as the slider motion is initiated but very steady repassivation occurs or the potential is gradually recovered to its original potential at the dwell period while the fretting motion of the slider is continued. The direct comparison of magnitude of potential drop between CoCrMo and Ti6Al4V clearly describe oxide chemistry. It is notable that the presence of the moderate acidic electrolyte with pH 4 is beneficial to both surfaces. Especially, it is presumable the fretting corrosion resistance of CoCrMo was significantly improved in sodium lactate pH 4. Repassivation of titanium surface also was

promoted in both of the initiation (onset) and progressive (active) stages of fretting. This results implies that the mechanical strength and rapid regrowth of Ti6Al4V superior to those of CoCrMo. The presence of lactate electrolyte improved the repassivation that is faster than metal ion dissolutions. After fretting stops, CoCrMo surface is rapidly re-passivated while Ti6Al4V was readily re-passivated during fretting motion. Therefore, the Ti6Al4V presented desirable oxide chemistry that recovers the damaged surface in the Lactate pH4 electrolyte.

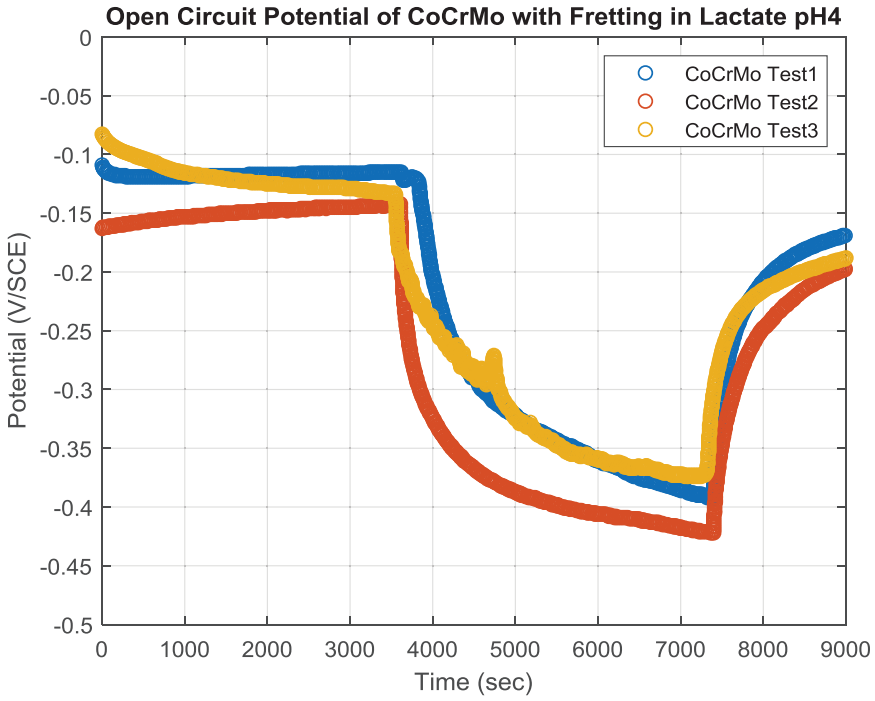

Figure 21: Graph of time vs potential of CoCrMo before fretting, during and after in sodium lactate pH4 solution

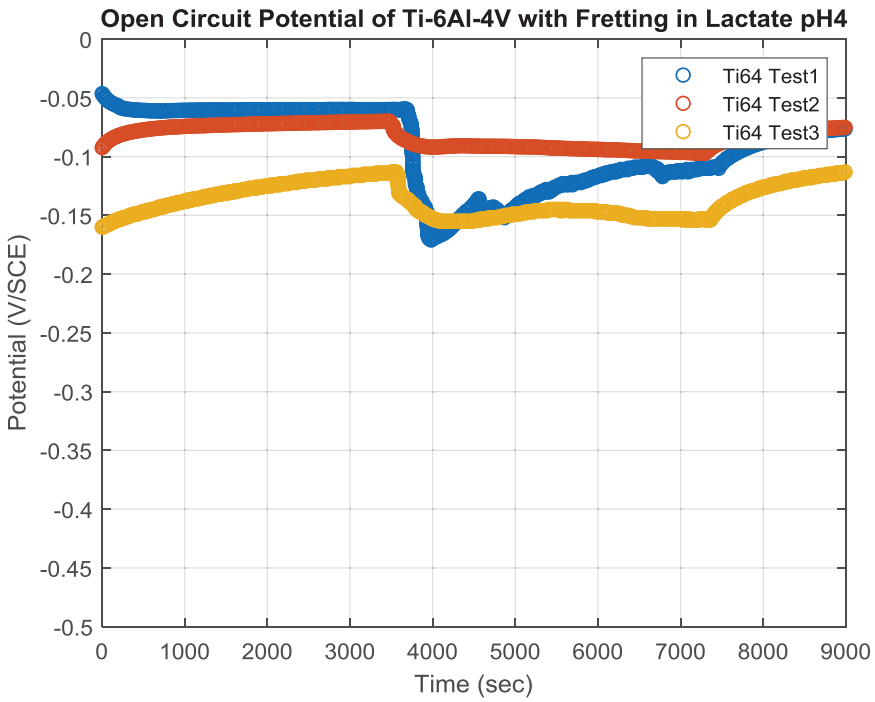

Figure 22: Graph of time vs potential of Ti6Al4V before fretting, during and after in sodium lactate pH4 solution

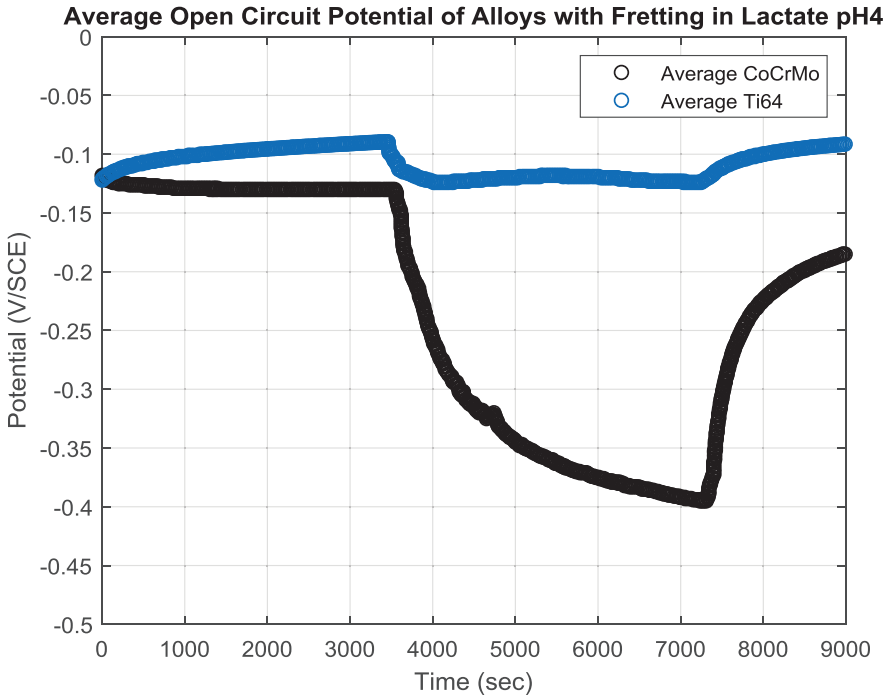

Figure 23: Average OCP on Ti6Al4V and CoCrMo in sodium lactate pH4 Solution

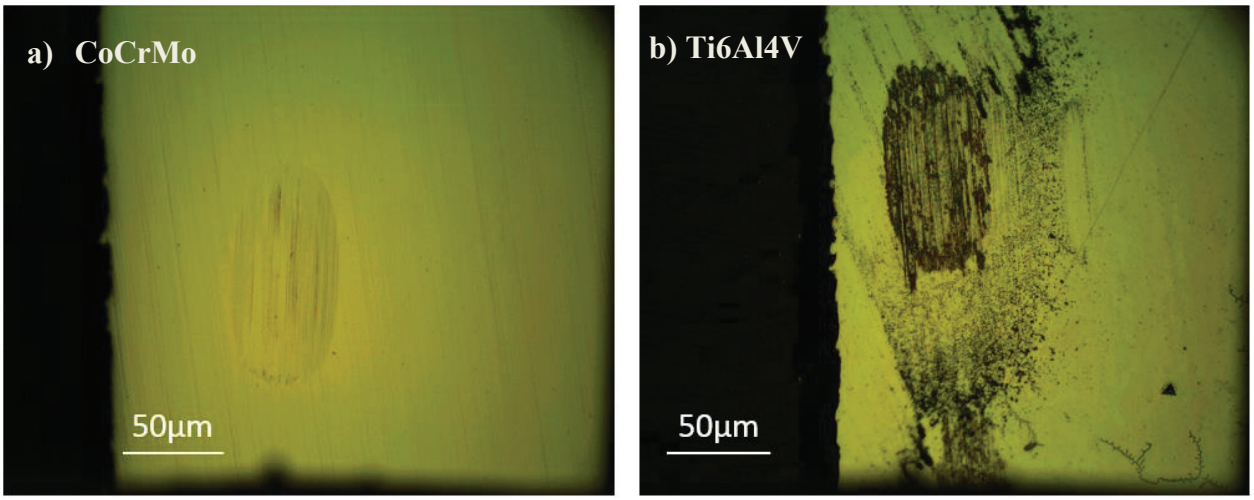

Figure 24: Optical microscope images of alloys in sodium lactate pH4. a) CoCrMo b) Ti6Al4V

Figures 25-26 shows changes in OCP at the onset and active fretting. As discussed, a dramatic drop in potential was observed when the fretting contact began on CoCrMo but not as significant in Ti6AL4V surface. However, the positive potential change obtained on Ti6Al4V also describes the spontaneous re-passivation of titanium oxide even during fretting. The oxidation chemistry on both surfaces triggered by fretting is less sensitive compared to PBS environment.

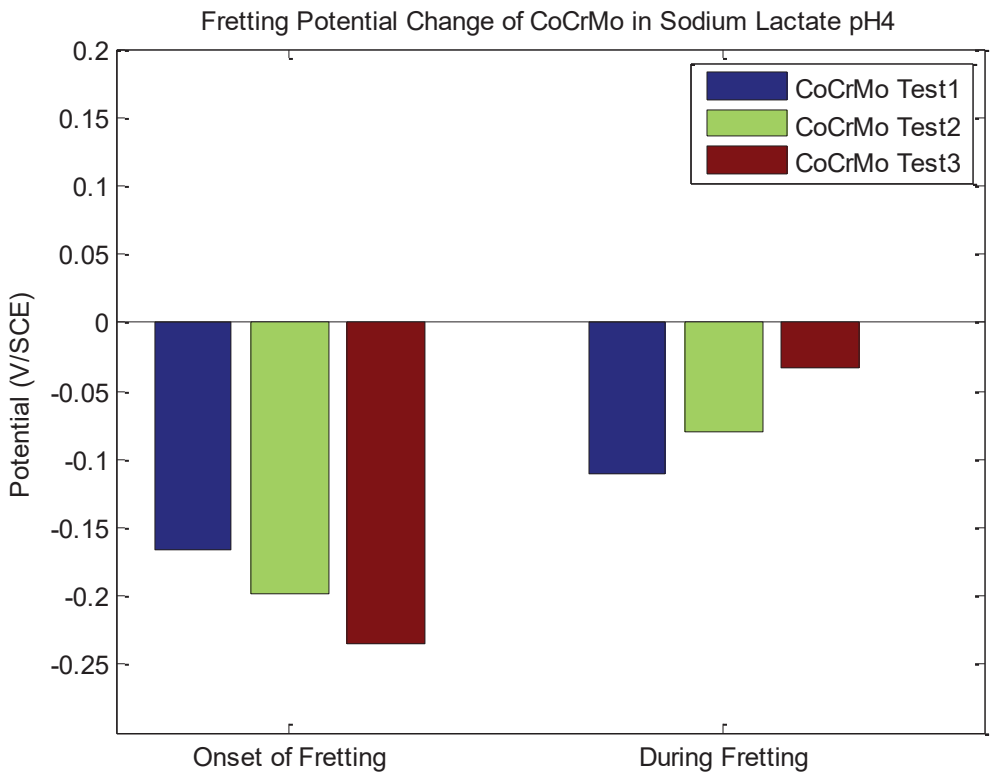

Figure 25: Statistical Analysis of OCP of CoCrMo Lactate pH4

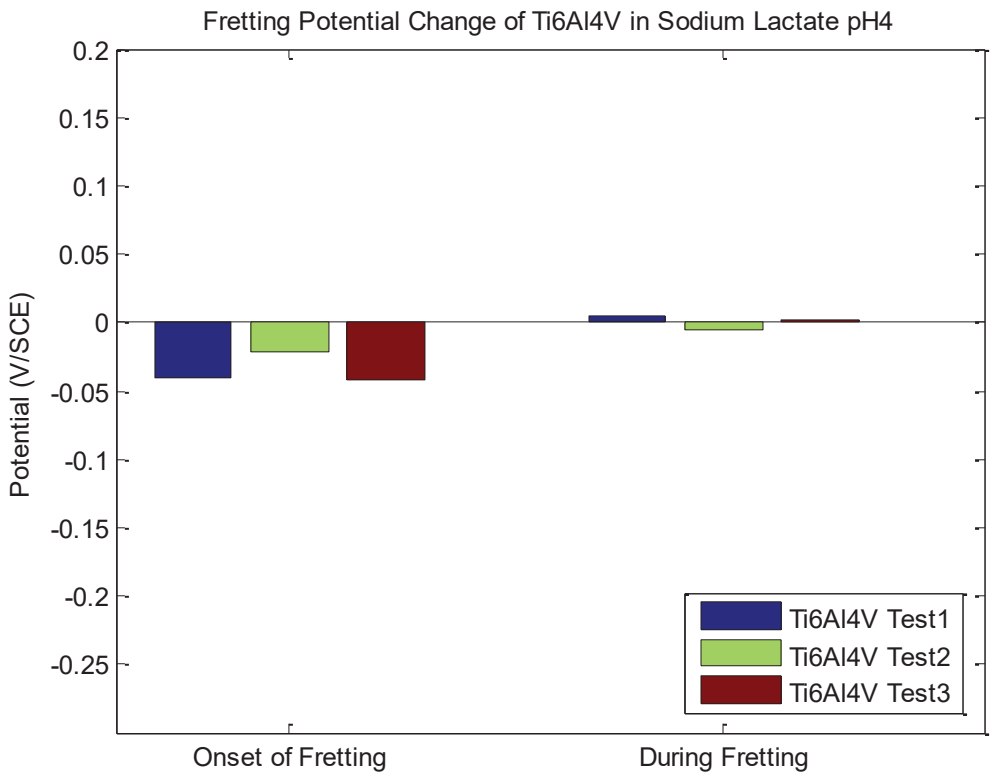

Figure 26: Statistical Analysis of OCP of Ti6Al4V Lactate pH4

However, friction responses are significantly modified with a change in environment/electrolyte as can be seen in figure 27-32. CoF values on CoCrMo reached a steady level of CoF, at about 0.5 though it was low to begin with in some instances. Throughout the entire fretting process, CoF values on CoCrMo is very stable and almost constant. This stable CoF values may be well explained by the micromorphology of wear damage. The nano debris progressively produced by fretting without complete spalling of breakage of the oxide layer. However, the stable CoF changes on Ti6AL4V is because of almost little to no delamination wear by fretting. Changes in OCP and CoF during microcracking is invisible. It is evident the fretting cycles at OCP drops is simultaneous with COF changes.

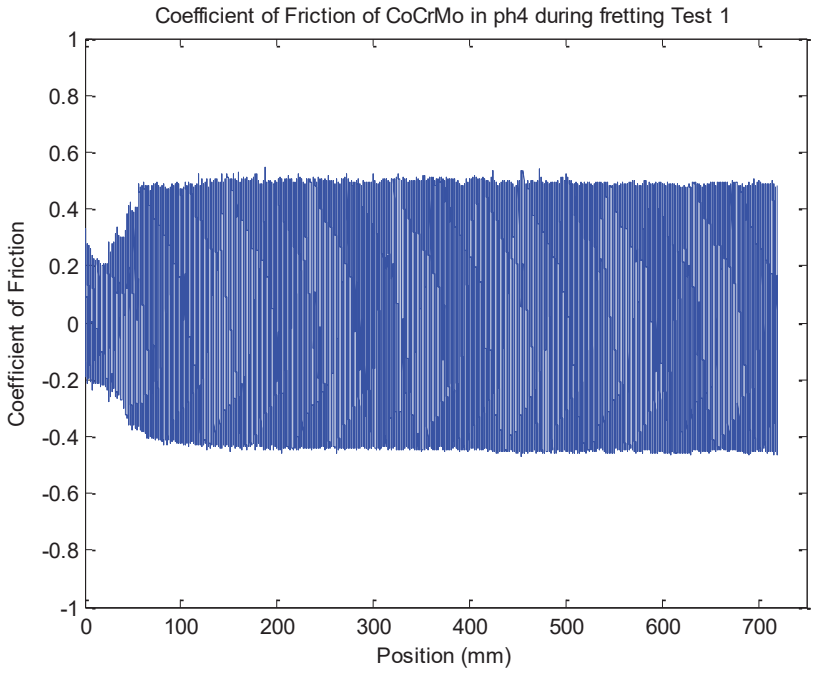

Figure 27: CoF plot of CoCrMo measurement in Lactate pH 4 Test 1

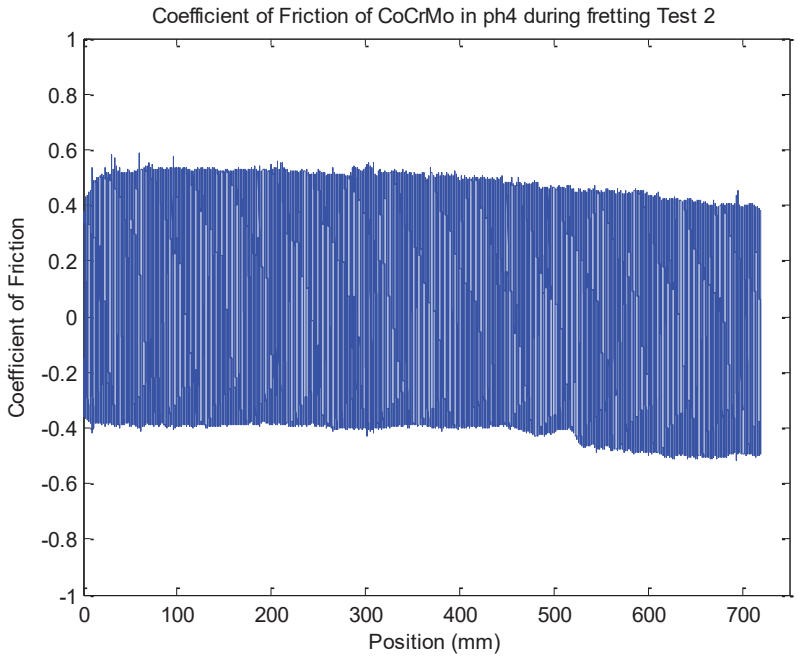

Figure 28: CoF plot of CoCrMo measurement in Lactate pH 4 Test 2

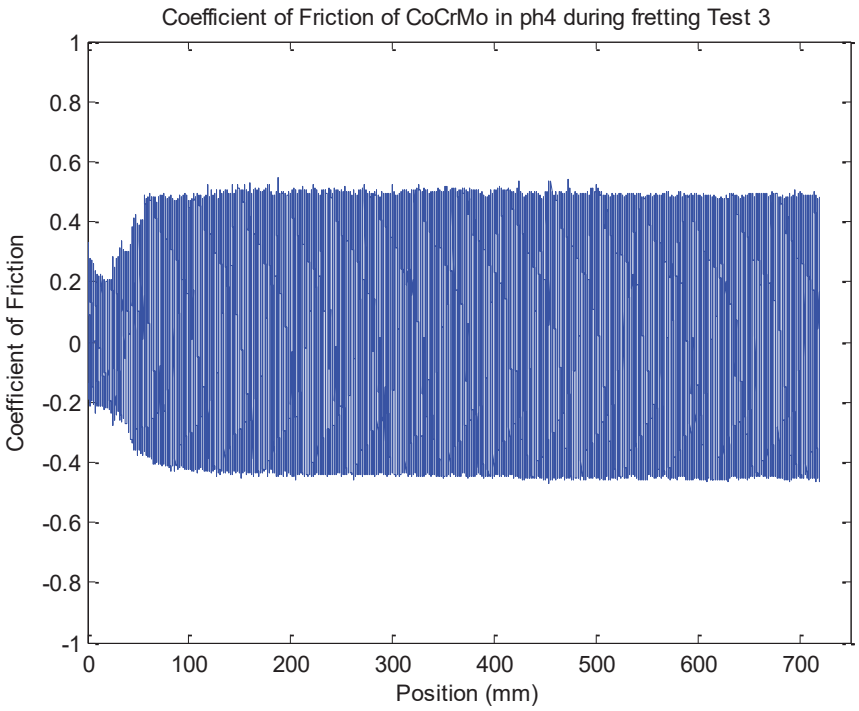

Figure 29: CoF plot of CoCrMo measurement in Lactate pH 4 Test 3

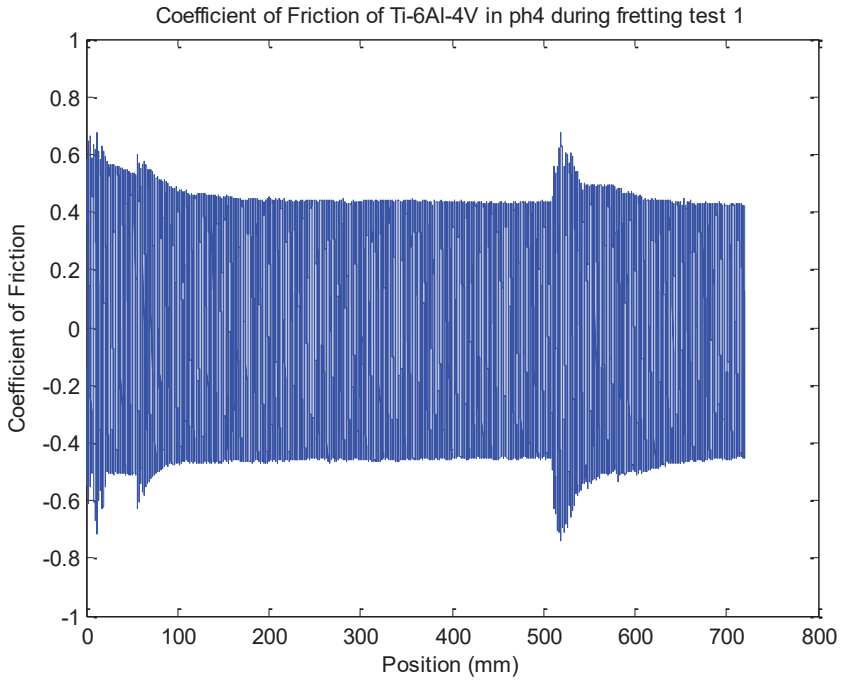

Figure 30: CoF plot of Ti6Al4V measurement in Lactate pH 4 Test 1

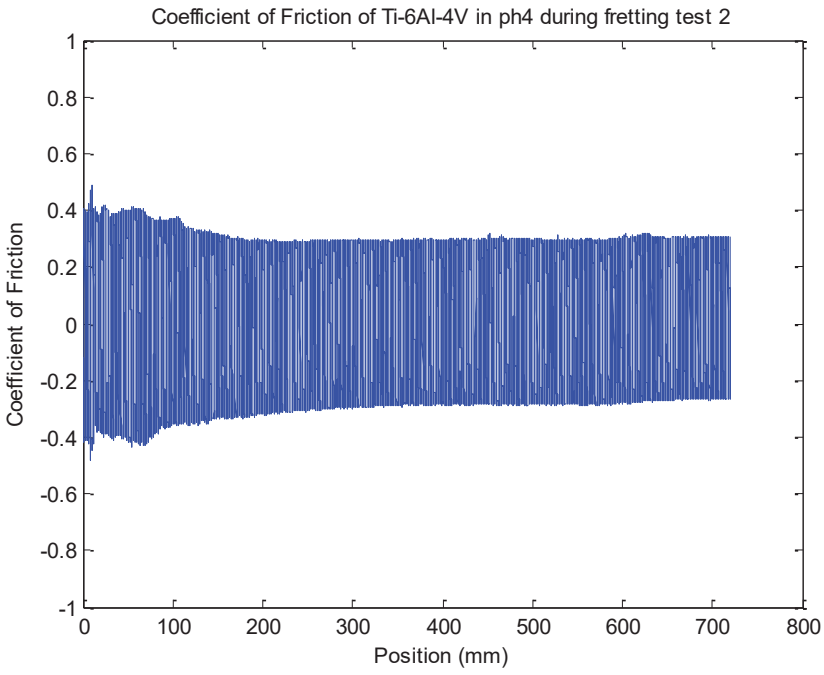

Figure 31: CoF plot of Ti6Al4V measurement in Lactate pH 4 Test 2

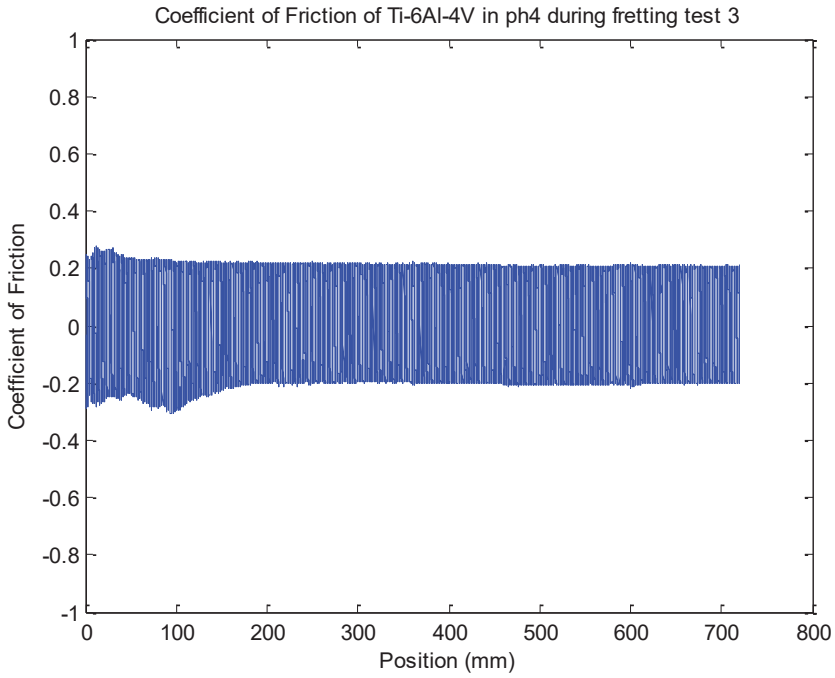

Figure 32: CoF plot of Ti6Al4V measurement in Lactate pH 4 Test 3

Table 11 shows the maximum and minimum values of CoF on the surface of the alloys during fretting in lactate pH4 solution. CoF values for both metals were high on the average in CoCrMo but lower in Ti6Al4V.

Table 11: Maximum and Minimum COF values in Lactate pH4 solution

Material	CoCrMo			Ti6Al4V ELI		
	Test 1	Test 2	Test 3	Test 1	Test 2	Test 3
Forward COF	0.51	0.58	0.37	0.64	0.27	0.41
Backward COF	-0.46	-0.52	-0.38	-0.68	-0.31	-0.42

4.3 Fretting Corrosion Test in Sodium Lactate pH 2 Solution:

The potential change by reciprocating motion with a constant normal load of 143mN was monitored before fretting (dwell), during fretting (active articulations) and after fretting motion (recovery) on CoCrMo and Ti-6A-4V. As shown in Figures 33-35, the potential was allowed to stabilize for an hour, and then the reciprocating motion using the spherical alumina was applied at 143mN. There was a significant potential drops on CoCrMo and Ti6Al4V surfaces due to the exposure of metal via a damaged oxide layer to a Lactate pH4 solution. However, the potential rapidly increased instantaneously and gradually increased during continuous fretting motions (Figure 33), while the potential of CoCrMo continually decreased until the fretting is ceased (Figure 34) that of Ti6Al4V instantaneously recovered during fretting. From the average potential drop by fretting contact compared in Figure 23, it is evident that the potential of Ti6Al4V significantly drops as soon as the slider motion is initiated but a spontaneous repassivation occurs and the potential is gradually recovered but not to its original potential as evident in PBS and Lactate pH4 at the dwell period while the fretting motion of the slider is continued. It is notable that the presence of the electrolyte is not as beneficial to titanium to reform its stable oxide layer compared to PBS and Lactate pH4. However, during fretting wear on CoCrMo the potential continuously drops until sliding motion is ceased after which it recovers at the halt of fretting. This shows that the mechanical strength of the reformed chromium oxide layer may not be comparable to the original passive layer formed in ambient. During fretting on CoCrMo surface's rapid fluctuation in potential shows repetition of deterioration-reformation of the oxide layer in Lactate pH2 [49]. A significant potential drop of Ti6Al4V in Lactate pH2 describes the effect the

electrolyte has on the ion oxidation to activate electrochemical reaction in the alloy. After fretting stops, CoCrMo surface is rapidly re-passivated while Ti6Al4V was readily re-passivated during fretting motion. Therefore, the Ti6Al4V presented desirable oxide chemistry that recovers the damaged surface in the Lactate pH4 electrolyte.

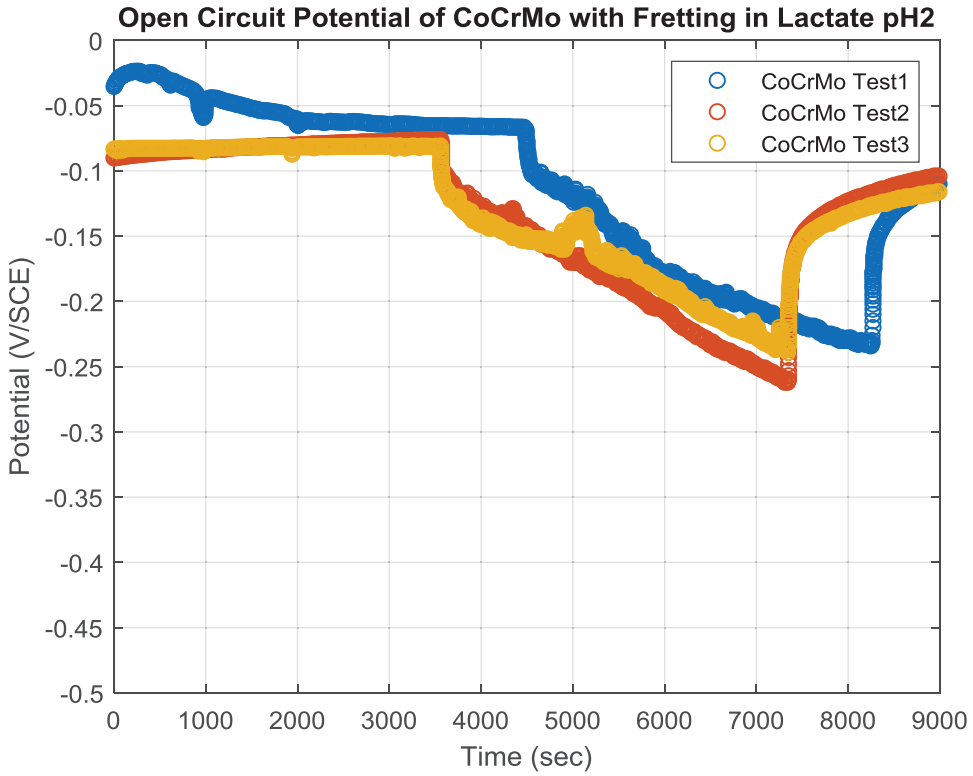

Figure 33: Graph of time vs potential of CoCrMo before fretting, during and after in Lactate pH2 solution

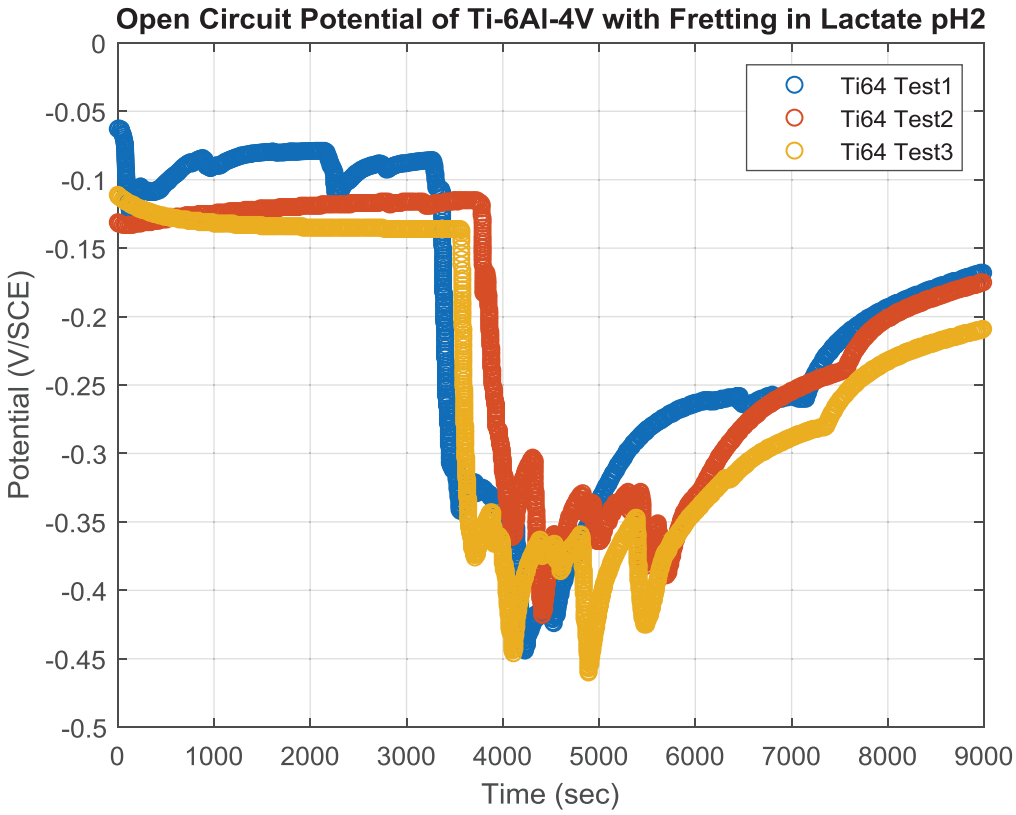

Figure 34: Graph of time vs potential of Ti6Al4V before fretting, during and after in Lactate pH2 solution

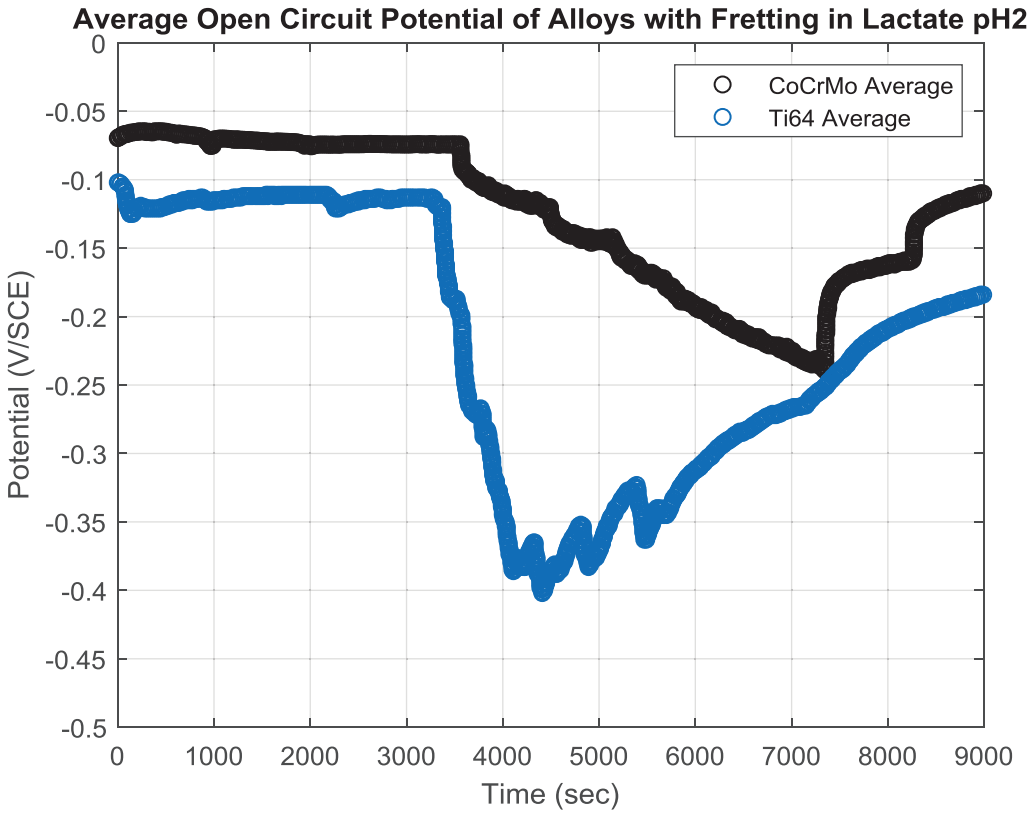

Figure 35: Average OCP on Ti6Al4V and CoCrMo in Lactate pH2 Solution

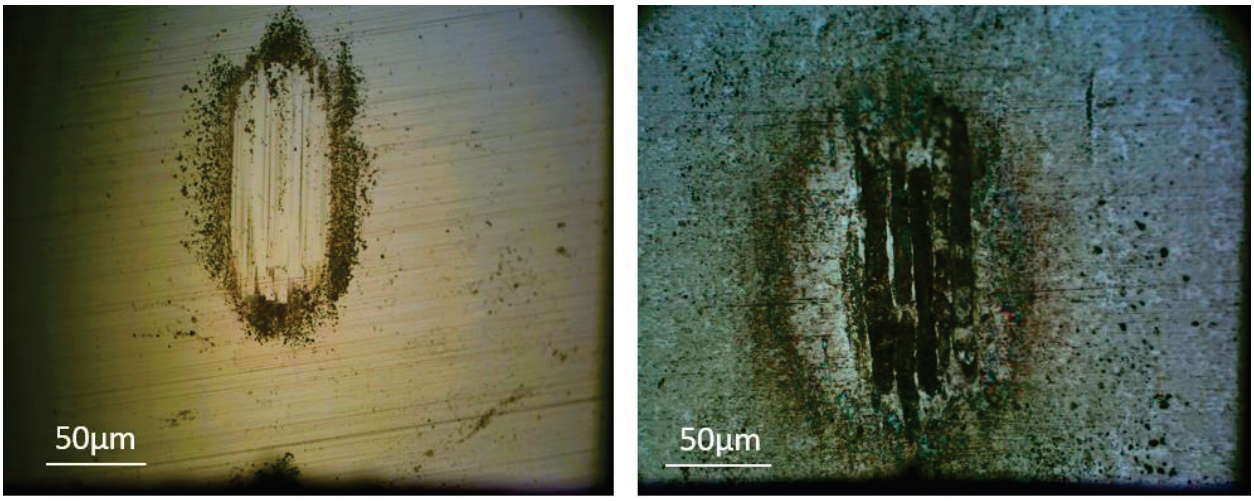

Figure 36: Optical microscope image of alloys in sodium lactate pH2 a) CoCrMo b) Ti6Al4V

The micro-morphologies on the damaged area by fretting in pH2 are different from those from fretting contact PBS. Especially, Ti6Al4V surface illustrated wear tracks by metal surface abrasion and largescale plastic strains. Wear damages on CoCrMo presents pile-up of nano debris mainly produced from progressive plowing of the oxide layer. Dark areas with undulations of grooves at Ti6Al4V are found, while the wear trench of CoCrMo is surrounded by small metal oxide wear particles. The wear of CoCrMo represents the corrosion debris composed mostly of oxide particles that are continuously formed on surface while scratching and removed from its place. The wear flakes produced by fatigue contact on Ti6Al4V surface would be crushed at the subsequent sliding contacts and amassed into fretting tracks. These oxide flakes are often removed from the contacting surface as the ball plows metal from Ti6Al4V. Due to this there are few more potential drops during OCP measurements. In CoCrMo less plastic deformation occurs leaving fretting marks are more visible. Changes in OCP at the onset of fretting and during fretting are summarized in figures 37-38. OCP drops on both CoCrMo and Ti6Al4V are significant when the fretting contact is initiated. However, the capability of oxide layer reformation on Ti6Al4V is much superior to that of CoCrMo during active sliding contact as evident by the positive potential values. The positive change in Ti6Al4V shows the degree of active re-passivation in lactate solution.

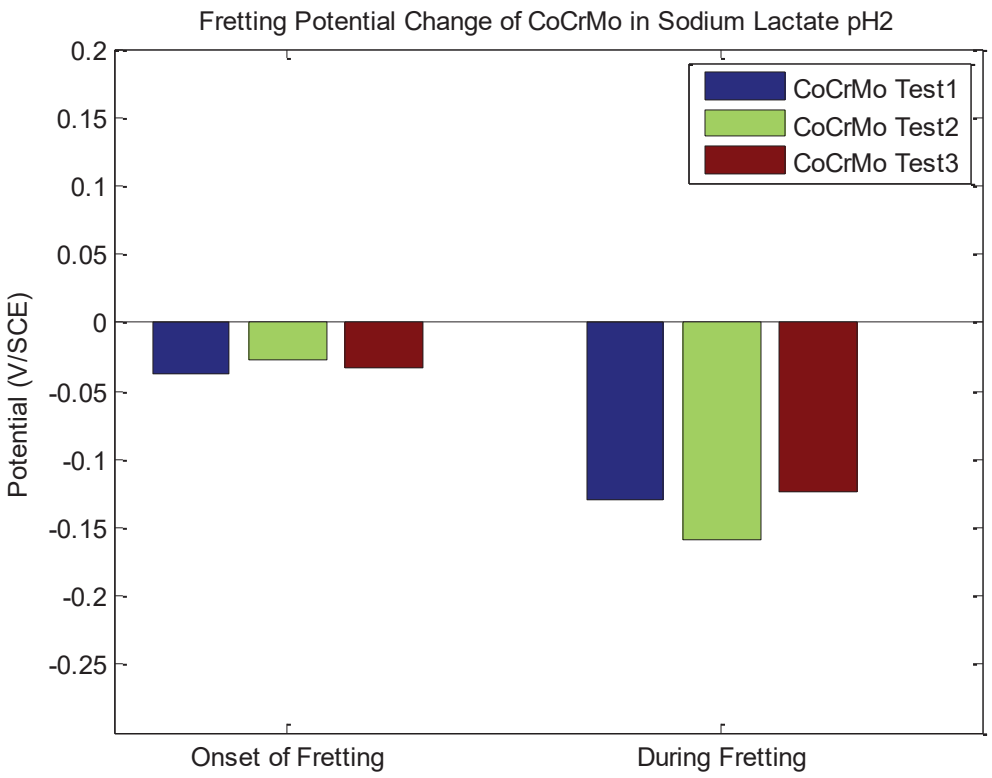

Figure 37: Statistical Analysis of OCP of CoCrMo in Lactate (pH2)

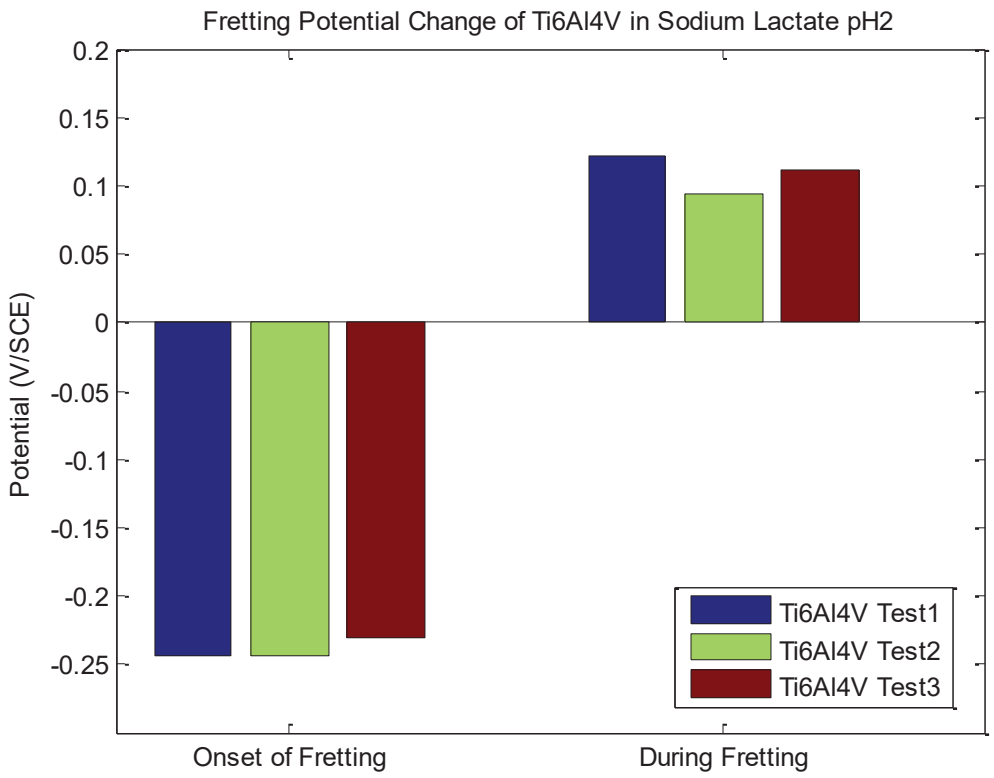

Figure 38: Statistical Analysis of OCP of Ti6Al4V in Lactate pH2

During its cumulated sliding distance, CoF values rapidly increase up to 0.3 in the early 250 cycles and then progressively stay stable during the entire fretting process as can be seen in figure 39-44. When the fretting is ceased, CoF values reach approximately 0.4. However, COF from Ti6Al4V surface illustrated more fractal behavior. The average CoF values on Ti6Al4V is smaller than those on CoCrMo, but the results present unstable friction response. As discussed in micromorphologies on the damaged area, the result suggests a cycle of CoF magnitude changes (alternating increase and decrease of CoF) is due to a repeated pattern of large abrasive wear debris formation and rejection. The wear debris will be subjected to a large scale plastic deformation and oxidation that result in agglomerated hard and brittle wear particles. During the following mechanical loadings, the brittle debris may induce third-body friction. Therefore, the result describes during the early fretting cycles mechanical loading significantly governs electrochemical

response, while later fretting cycles the recovered oxide layer stabilizes the tribological response of the Ti6Al4V surface.

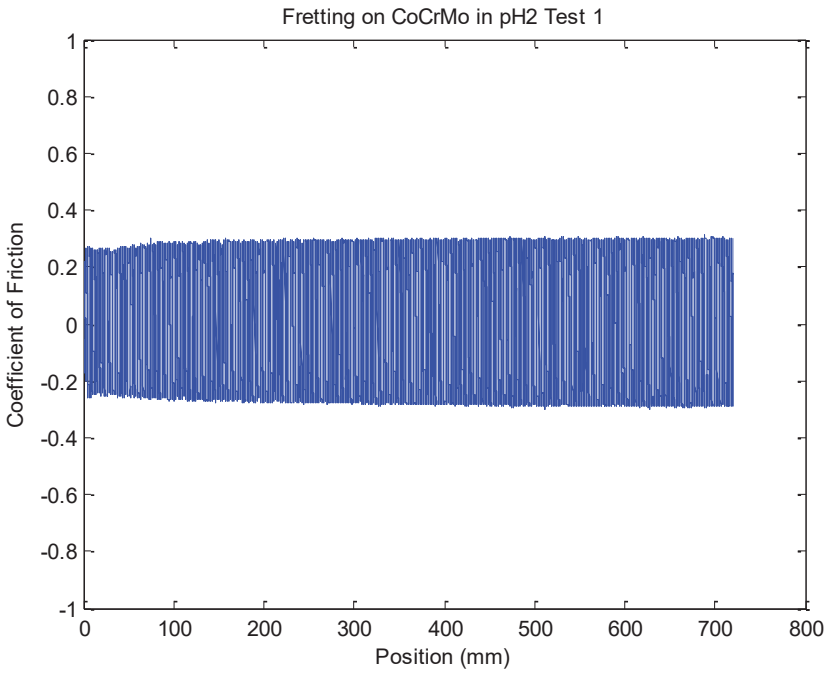

Figure 39: CoF plot of CoCrMo measurement in Lactate pH2 Test 1

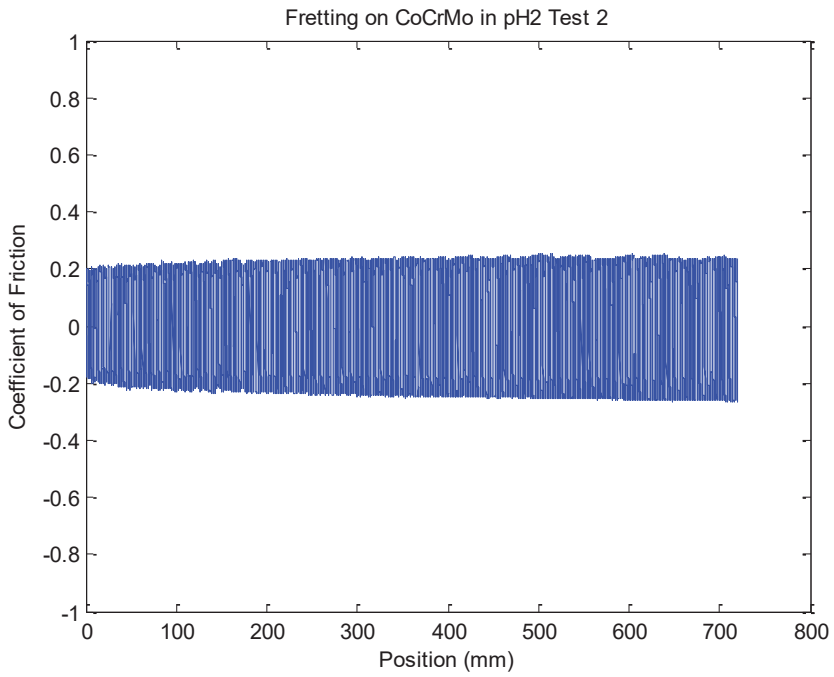

Figure 40: CoF plot of CoCrMo measurement in Lactate pH2 Test 2

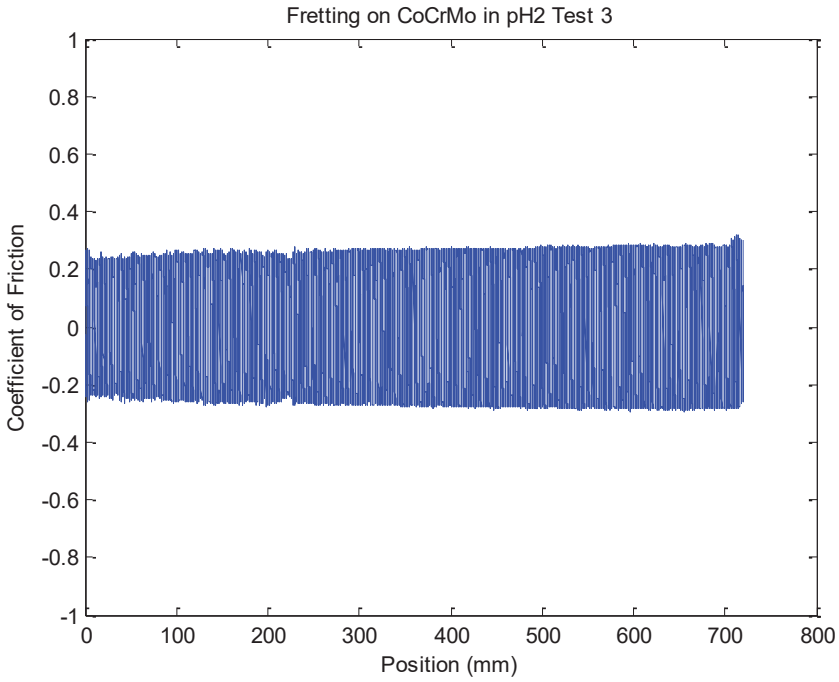

Figure 41: CoF plot of CoCrMo measurement in Lactate pH 2 Test 3

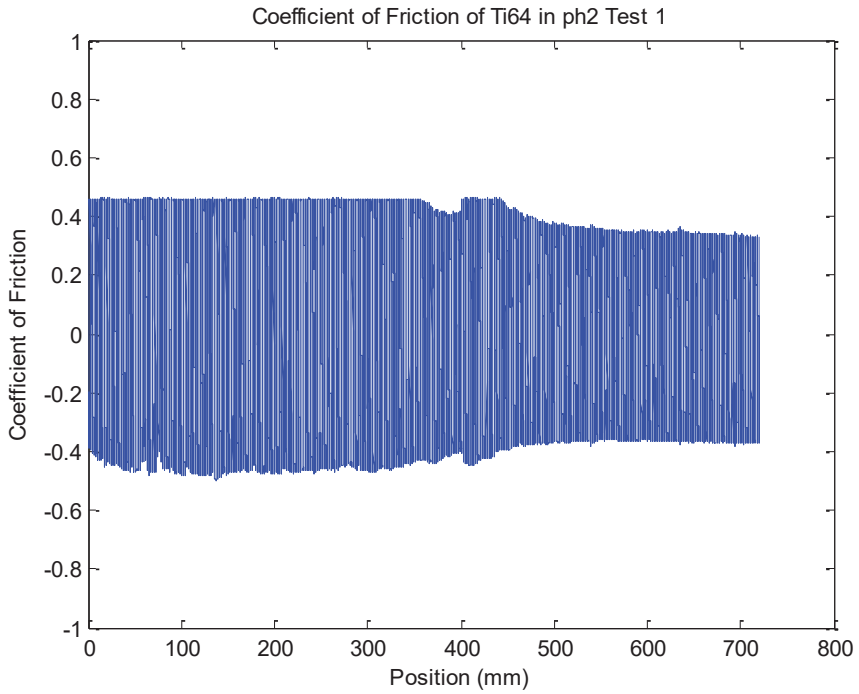

Figure 42: CoF plot of Ti6Al4V measurement in Lactate pH 2 Test 1

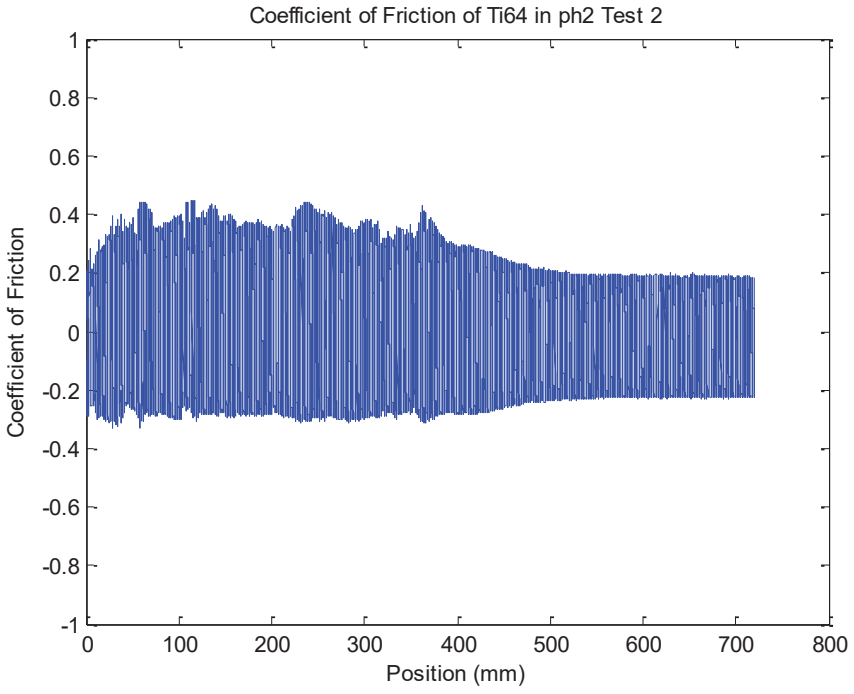

Figure 43: CoF plot of Ti6Al4V measurement in Lactate pH 2 Test 2

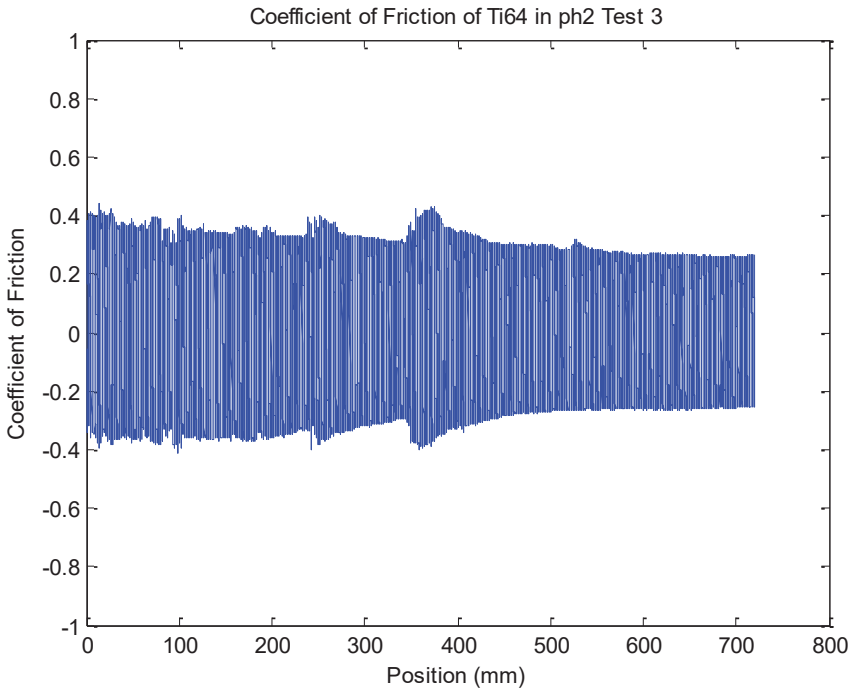

Figure 44: CoF plot of Ti6Al4V measurement in Lactate pH 2 Test 3

Table 12 shows the maximum and minimum values of CoF of Ti6Al4V and CoCrMo in Lactate pH2. COF values for both metals were low in this electrolyte.

Table 11: Maximum and Minimum COF values in Lactate pH2 Solution

Material	CoCrMo			Ti6Al4V		
	Test 1	Test 2	Test 3	Test 1	Test 2	Test 3
Forward COF	0.30	0.24	0.43	0.46	0.42	0.44
Backward COF	-0.30	-0.27	-0.46	-0.49	-0.35	-0.33

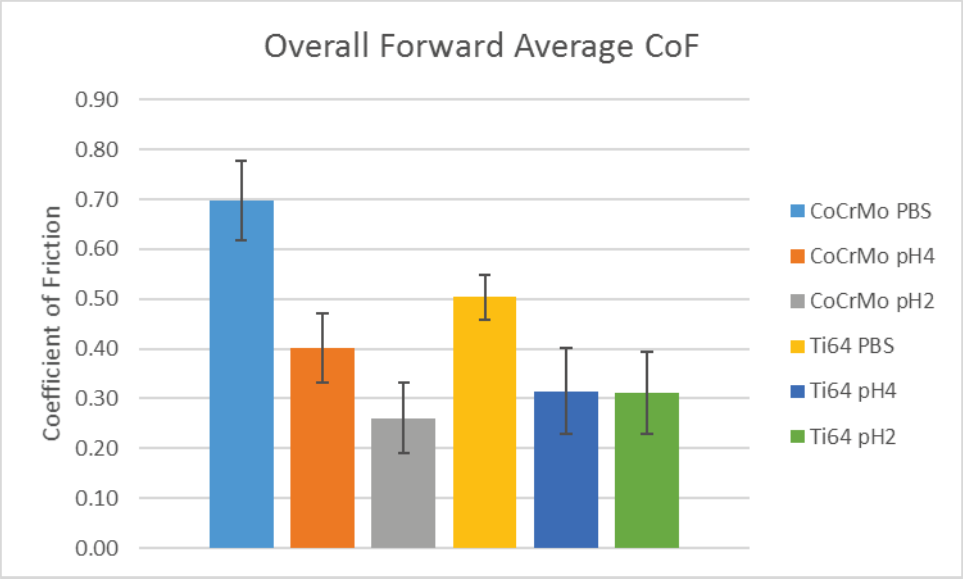

Figure 45: Overall Average Forward CoF of Ti-6Al4V and CoCrMo in PBS (pH7.4), Lactate (pH4 and pH2)

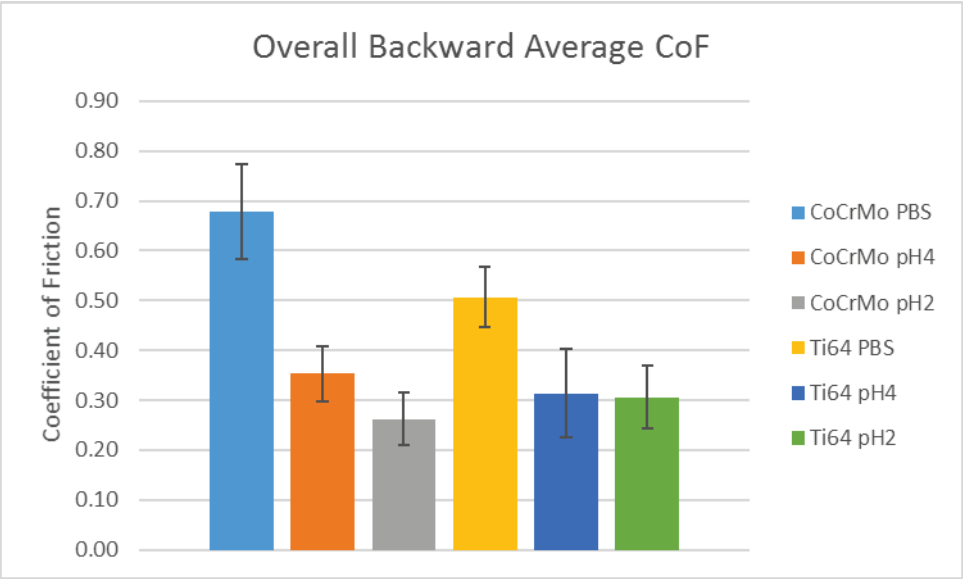

Figure 46: Overall Average Backward CoF of Ti-6Al4V and CoCrMo in PBS (pH7.4), Lactate (pH4 and pH2)

4.4 Potentiostatic Polarization

Potentiostatic Polarization tests were performed at three potential voltages at -0.6, 0.0, and +0.6 V in all three inflammatory environments on both alloys during fretting contact using the parameters as explained in the experimental procedure. Figure 47 is a representation of current density change against potentials applied to CoCrMo in PBS and Lactate pH4 during fretting contact. During the test, the current was allowed to stabilize at values known as baseline current density (up to 900 seconds before fretting began). The baseline current is dependent on the surface condition of the alloy during the time of test and the electrolyte. The current values change from negative to positive when applied potentials from negative to positive. However, the current does not change in Lactate pH4 but in PBS it does during fretting throughout the test period. Therefore, the PBS solution induces a significant oxidation oxidation of ions on CoCrMo surface at the given voltage (0.6V). This result is in accordance with the micromorphology of the damaged area as illustrated in Figure 12.

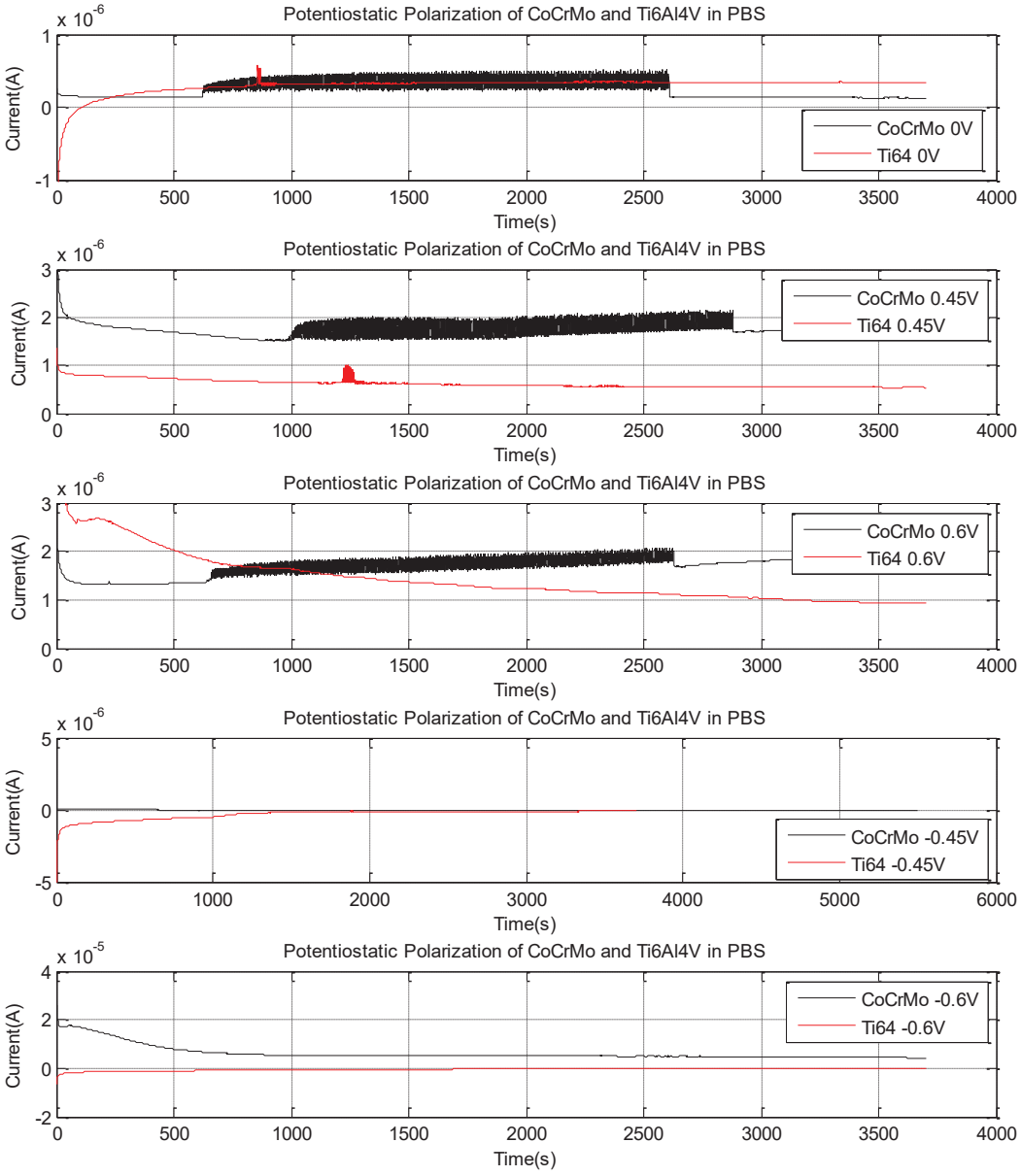

Figure 47: Potentiostatic Polarization of CoCrMo and Ti6Al4V in PBS at 0, 0.45, 0.6, -0.45 and -0.6V

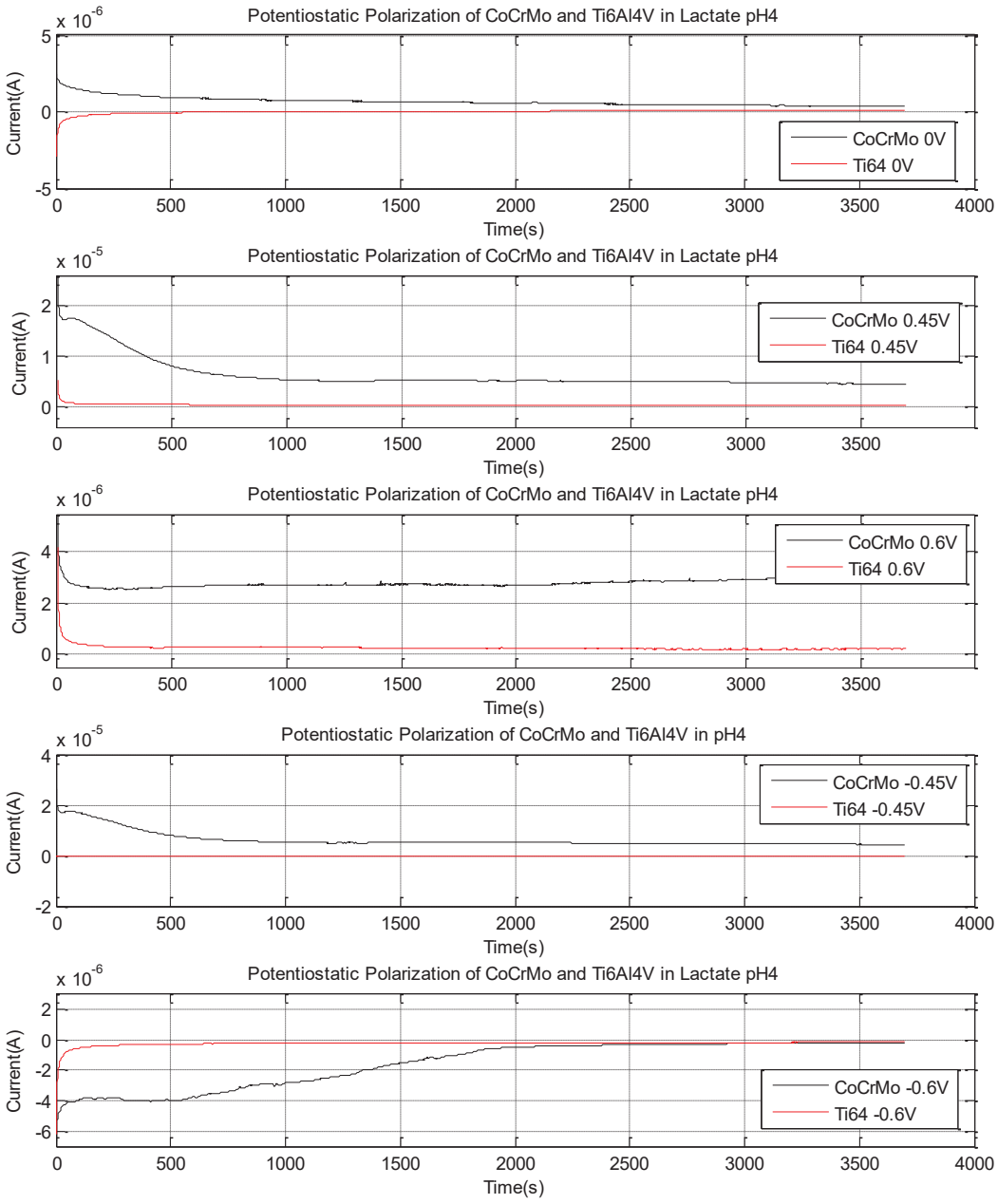

Figure 48: Potentiostatic Polarization of CoCrMo and Ti6Al4V in Sodium Lactate pH4 at 0, 0.45, 0.6, -0.45 and -0.6V

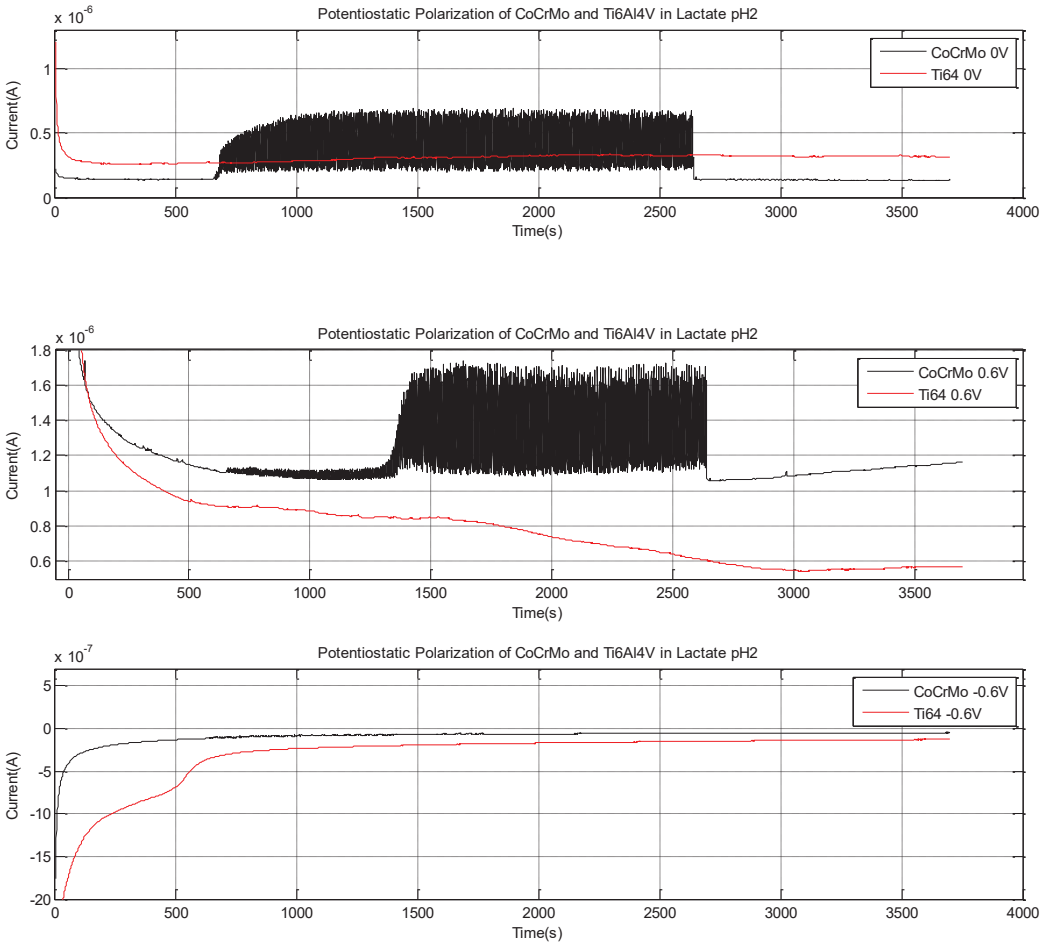

Figure 49: Potentiostatic Polarization of CoCrMo and Ti6Al4V in Lactate pH2 at 0, 0.6 and -0.6V

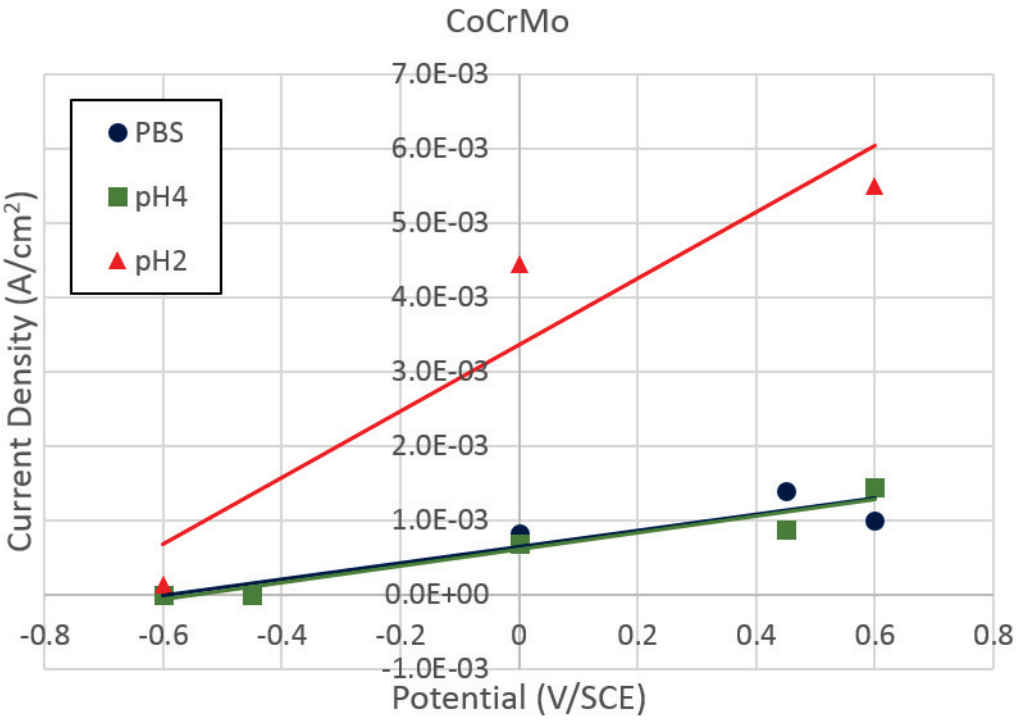

Figure 50: Statistical Analysis of Potentiostatic Test on CoCrMo

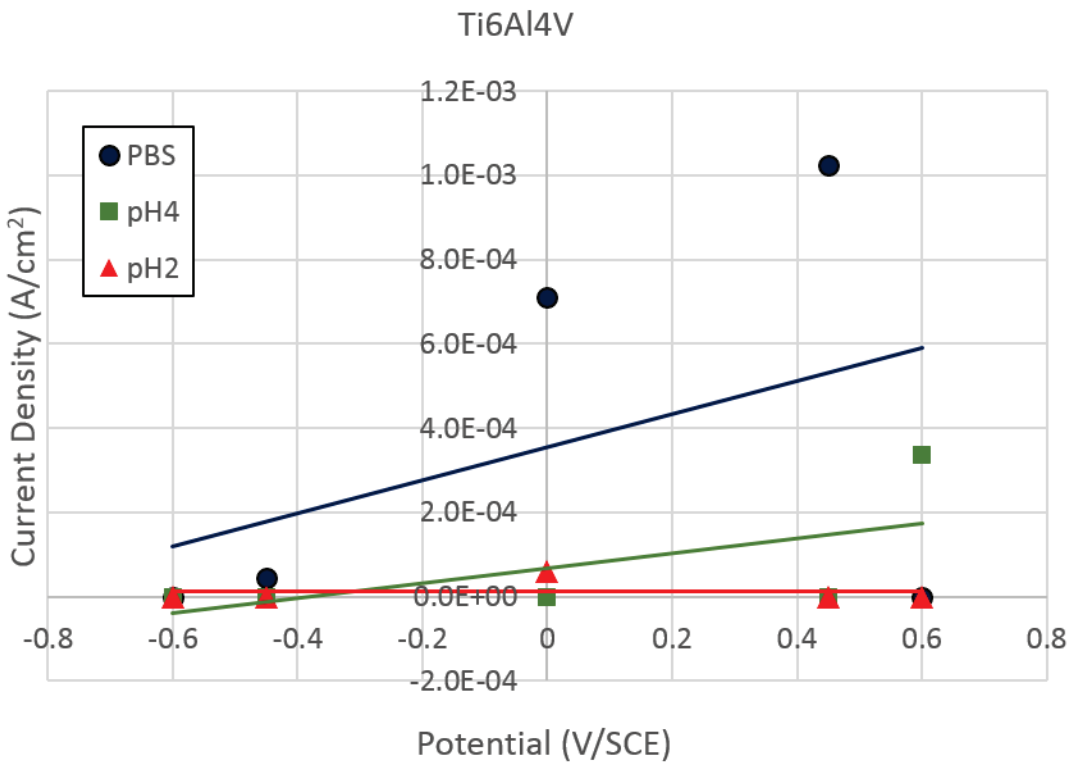

Figure 51: Statistical Analysis of Potentiostatic Test on Ti6Al4V

A series of current density measurement was performed on Ti6Al4V at potential values 0, 0.45, 0.6, -0.45 and 0.6V. All the results presented in Figures 47-49 show no current change at all potentials and electrolytes. The results prove that the oxidation chemistry of titanium is not sensitive against electrochemical or mechanical stimuli. It may conclude Ti6Al4V implants would be superior in tribocorrosion damage process.

Current density evolution of two surfaces as a function of applied potentials is summarized in Figures 50-51 represents. A statistical representation of Potentiostatic illustrated the active metal dissolution takes place on CoCrMo surface with the significant increase in current in both sodium lactate pH2 and PBS at and while the electrochemical response of Ti6Al4V would be stable in the mechanical and chemical combinations.

Chapter 5: Conclusion

In conclusion, this study investigated two commonly used metallic hip implant materials in simulated synovial environments to compare the effects of variable chemical environments on wear mechanism of two different metal alloys. This investigation was carried out using two methods; Potentiostatic polarization and open circuit potential measurements using a nanoindenter-based wear test combined with a potentiostat device. Experimental results illustrated that during fretting, there is a gradual drop in the potential of the CoCrMo alloy which signifies depletion of the chromium oxide layer until fretting ceases. After fretting the potential rapidly increased which implies the protective metal oxide layer was quickly regained. The results on Ti6Al4V, there is a significant potential drop followed by an almost immediate recovery of its oxide layer even during the continuous fretting motions. This result described spontaneous improvement of titanium oxide layer against mechanical and electrochemical stimuli.

Mechanical responses were monitored by observing changes in CoF values throughout fretting tests. CoCrMo surface showed greater CoF values and their variations, while Ti6Al4V less CoF values as well as more stable friction forces applied during fretting in PBS solution. In sodium lactate with both pH 4 and pH 2 conditions, the CoF values for both of the CoCrMo and Ti6Al4V surfaces were significantly reduced. However, Ti6Al4V surface presented the less sensitivity of CoF against pH levels in acidic conditions: the average CoF values on Ti6Al4V are almost identical in both pH 4 and pH 2 sodium lactate environments, while CoF values on CoCrMo reduces with the degree of acidity. This wear process would be explained that the nanoscale abrasion of chromium oxide layer increased CoF values. The less CoF values of Ti6Al4V would be explained by the OCP changes: the protective oxide layer was rapidly recovered even during active fretting attacks. The reformed hard titanium oxide reduces CoF values. Furthermore, this also proves that during fretting, the synovial environment plays a vital role in tribological responses on CoCrMo implants and the progressive re-passivation on Ti6Al4V stabilizes the tribological response during fretting attacks.

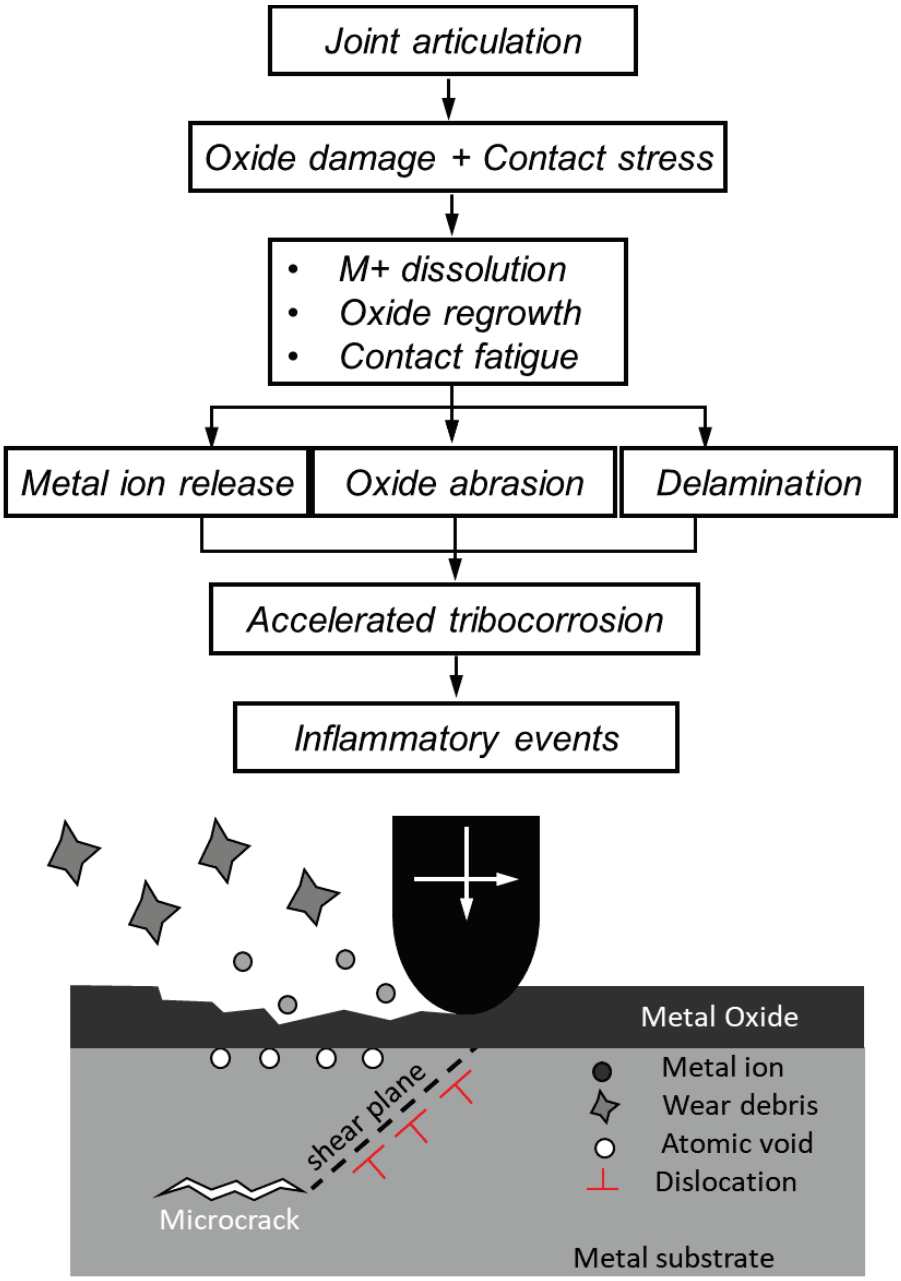

Figure 52: The Tribocorrosion process on metallic implant surface

The potentiostatic polarization test results of the CoCrMo alloy illustrated significant changes in its current in PBS and sodium lactate pH 2 electrolyte, while in Ti6Al4V fretting current change was not clear. This may imply the increase in ion concentration in the electrolyte from the dissolution of ions on the surface of the metal during fretting. Figure 48 summarizes the tribocorrosion process on the surface of the metal. Consequently, the dominant wear mechanisms

would be oxide layer abrasion of CoCrMo versus delamination wear of Ti6Al4V. The mechanical energy by fretting contact was consumed by oxide layer abrasion on CoCrMo, while the greater plastic strain on Ti6Al4V accelerates repassivation to protect the surface against subsequent electrochemical dissolutions.

Therefore, the Ti6Al4V alloy is superior in terms of tribocorrosion as compared to the CoCrMo alloy even though CoCrMo has superior mechanical strengths. To conclude, Ti6Al4V is a better implant material than CoCrMo alloy.

This thesis aided in answering some question regarding the tribocorrosion of two most commonly used metal alloys in the biomedical department. It also helped answer questions regarding which is less harmful to the human body but it is imperative that further research is done to further support the above conclusions. Listed below are a few;

- Conducting the experiments in a more alkaline region thus in this case an alcoholic patient with a hip implant.
- Increasing testing time, scratch length and speed. Increase in speed will mean the rate of deterioration in an athlete.
- Use of confocal imaging to better capture the wear rate of the metal under fretting.
- Use of other electrochemical tests such as Potentiodynamic Polarization.

REFERENCES

[1] *Annual Reports*. Retrieved July 15, 2019, from http://www.ajrr.net/publications-data/annual-reports.

[2] Yan, Y. (2013). *Bio-tribocorrosion in biomaterials and medical implants*. Oxford. Pg. 74-79.

[3] Rosenberg A. Bones, joints, and soft tissue tumors. In: Cotran RS, Kumar V, Collins, T, eds. *Robbins Pathologic Basis of Disease*. 6th ed. Philadelphia, PA: WB Saunders Co; 1999:1253.

[4] *"Hip Replacement Materials - A Complete Guide to the Best and Worst."* [Online]. Available: https://www.regenexx.com/blog/research/hip-replacement-materials---a-complete-guide-to-the-best-and-worst/. [Accessed: 20-Nov-2018].

[5] *Hip Replacement Implant Materials*. Retrieved July 15, 2019, from https://bonesmart.org/hip/hip-replacement-implant-materials/

[6] Moharrami, N., Langton, D.J., Sayginer, O. et al., *Thin Solid Films,* 549: 79-86, 2013

[7] Langton D.J., Sidaginamale, R., Lord, J.K. et al. *Bone Joint, Res.* 56:1, 2012.

[8] *OpenStaxCollege*. (2012, January 23). Retrieved May 21, 2019, from https://opentextbc.ca/physicstestbook2/chapter/friction/

[9] *Friction*. Retrieved July 15, 2019, from https://www.virginia.edu/ep/SurfaceScience/friction.html

[10] S. Glyn-Jones, H. Pandit, Y.-M. Kwon, H. Doll, H. S. Gill, and D. W. Murray, *"Risk factors for inflammatory pseudotumour formation following hip resurfacing," J. Bone Joint Surg. Br.*, vol. 91-B, no. 12, pp. 1566–1574, Dec. 2009.

[11] Kim, W. H.; Laird, C. (1978). *"Crack nucleation and stage I propagation in high strain fatigue—II. mechanism".* Acta Metallurgica. **26** (5): 789–799. doi:10.1016/0001-6160(78)90029-9

[12] Brubaker, G., R., Phipps, P., Beverley, &. (1979). *Corrosion chemistry*.

[13] *"In vitro simulation of fretting-corrosion in hip implant modular junctions: The influence of pH."* Royhman D, Patel M, Jacobs JJ,Wimmer MA, Hallab NJ, Mathew MT. Med Eng Phys. 2018 Feb

[14] Fontana, M. G. and Greene, N. D. *Corrosion Engineering. Electrochemistry and Corrosion.* McGraw-Hill, New York, N.Y., 1967.

[15] Compte, P. (1984). *Metallurgical observations of Biomaterials. In Contemporary Biomaterials,* J. W. Boretos and M. Eden, eds. Noyes Publ., Park Ridge, NJ, pp. 66-91.

[16] *Electrochemical Techniques in Corrosion Engineering*, National Association of Corrosion Engineers, 1986

[17] J.B. Park, R.S. Lakes, *Biomaterials: An Introduction*, Springer, New York, 2007.

[18] *Biomaterials*. (2017, October 25). Retrieved from https://www.nibib.nih.gov/science-education/science-topics/biomaterials.

[19] Pavlovic, M. (2015). *Bioengineering: A conceptual approach*. Cham: Springer. Pg. 229.

[20] Barbero, E. J. (1998). *Introduction to Composite Materials Design*. Taylor and Francis, Philadelphia.

[21] Ratner, B. D. (2011). *Biomaterials science: An introduction to materials in medicine*. Amsterdam: Elsevier, Acad. Press. Pg. 138

[22] Gilbert JL. *Electrochemical behavior of metals in the biological milieu*. In: Healy KE, Ducheyne P, Kirkpatrick CJ, editors. Comprehensive Biomaterials. Elsevier Press; Chapter 13; 2011

[23] Megremis SJ. *The mechanical, electrochemical, and morphological characteristics of passivating oxide films covering cobalt-chromium-molybdenum alloys: A study of five microstructures*. Ph.D thesis, Northwestern University. 2001.

[24] Compte, P. (1984). *Metallurgical observations of Biomaterials. In Contemporary Biomaterials*, J. W. Boretos and M. Eden, eds. Noyes Publ., Park Ridge, NJ, pp. 66-91.

[25] Beevers, C. J., and Robinson, J. l. (1969). *Some observations on the influence of oxygen content on the fatigue behavior of α-titanium*. J. Less-Common Metals 17: 345-352.

[26] *Industrial/Training Services - DM&ME*. Retrieved July 15, 2019, from http://www.dmme-engineering.com/industrialtraining-services/

[27] *Standard Terminology Relating to Wear and Erosion, Annual Book of Standards, Vol 03.02*, ASTM, 1987, p 243-250.

[28] Lipsitt, H. A., and Wang, D. Y. (1961). *The effects of interstitial solute atoms on the fatigue limit behavior of titanium*. Trans. AIME 221: 918.

[29] Barbero, E. J. (1998). *Introduction to Composite Materials Design*. Taylor and Francis, Philadelphia.

[30] Marcus, P. (2011). *Corrosion Mechanisms in Theory and Practice, Third Edition*. CRC Press.

[31] Fontana, M. G. and Greene, N. D. *Corrosion Engineering. Electrochemistry and Corrosion*. McGraw-Hill, New York, N.Y., 1967.

[32] *Electrochemical Techniques in Corrosion Engineering*, National Association of Corrosion Engineers, 1986

[33] *Online Tutorials | School of Materials Science and Engineering*. Retrieved July 15, 2019, from http://www.materials.unsw.edu.au/tutorials/online-tutorials

[34] Agarwal, B. D., and Broutman, L. J. (1980). *Analysis and Performance of Fiber Composites*. Wiley-Interscience, New York.

[35] *Hip Replacement Materials – A Complete Guide to the Best and Worst*. Retrieved July 15, 2019, from https://regenexx.com/blog/hip-replacement-materials-best-worst/

[36] Askeland, Donald R.; Phulé, Pradeep P. (2006). *The science and engineering of materials* (5th ed.). Cengage Learning. p. 198. ISBN 978-0-534-55396-8. Elastic modulus

[37] Reiner, Markus (1943), *Ten Lectures on Theoretical Rheology*, Jerusalem: Rubin Mass, p. 137. Yield strength

[38] *"Generic MMPDS Mechanical Properties Table"*. *stressebook.com*. 6 December 2014. Archived from the original on 1 December 2017. Retrieved 27 April 2018. Ultimate tensile strength

[39] Courtney, Thomas (2005). *Mechanical Behavior of Materials*. Chapter 9: Waveland Press. pp. 433–436. ISBN 1-57766-425-6. Fracture toughness

[40] Campbell, Flake C. (2008). *Elements of Metallurgy and Engineering Alloys*. ASM International. p. 206. ISBN 9780871708670. Modulus of resilience

[41] Beer, Ferdinand P.; E. Russell Johnston, Jr. (1992). *Mechanics of Materials* (2 ed.). McGraw-Hill, Inc. p. 51. ISBN 978-0-07-837340-4. Endurance limit

[42] *Surface Modification of Ti-6Al-4V By Electrochemical*. Retrieved July 15, 2019, from https://pdfs.semanticscholar.org/164a/95a1f13bb9b513fb1ddd836661a322856efb.pdf

[43] *Studies on Titanium Hip Joint Implants using Finite Element Simulation*. Retrieved July 15, 2019, from http://www.iaeng.org/publication/WCE2016/WCE2016_pp986-990.pdf.

[44] K. Wang, *The use of titanium for medical applications in the USA*, Mat. Sci. Eng. A213 (1996) 134-137.

[45] Baron, S., Desmond, D., & Ahearne, E. (2019). *The fundamental mechanisms of wear of cemented carbide in continuous cutting of medical grade cobalt chromium alloy (ASTM F75). Wear,424-425*, 89-96. doi:10.1016/j.wear.2019.01.096

[46] Bhushan, B. (2013). *Principles and Applications of Tribology*. John Wiley & Sons.

[47] *Friction*. (n.d.). Retrieved from http://hyperphysics.phy-astr.gsu.edu/hbase/frict.html

[48] *Wear*. (2019, April 16). Retrieved June 13, 2019, from *https://en.wikipedia.org/wiki/Wear*.

[49] Chattopadhyay, R. (2001). *Surface Wear - Analysis, Treatment, and Prevention*. OH, USA: ASM-International. ISBN 978-0-87170-702-4

[50] Totten, G., E., & Liang, H. (2004). *Surface Modification and Mechanisms*. CRC Press.

[51] Akchurin, Aydar; Bosman, Rob; Lugt, Piet M.; Drogen, Mark van (2016-06-16). *"Analysis of Wear Particles Formed in Boundary-Lubricated Sliding Contacts"*. *Tribology Letters*. **63** (2): 16. doi:10.1007/s11249-016-0701-z. ISSN 1023-8883

[52] MacQuarrie, R.A., Chen, Y.F., Coles, C., Anderson, G.I.: *Wearparticle–induced osteoclast osteolysis: the role of particulates and mechanical strain*. J. Biomed. Mater. Res. B Appl. Biomater. 69B, 104–112 (2004)

[53] Biomaterials 19, 2297–2302 (1998), Elfick, A.P.D., Green, S.M., Krickler, S., Unsworth, A.: *The nature and dissemination of UHMWPE wear Debris retrieved from periprosthetic tissue of THR*. J. Biomed. Mater. Res. 65A, 95–108 (2003)].

[54] *Standard Terminology Relating to Wear and Erosion, Annual Book of Standards, Vol 03.02*, ASTM, 1987, p 243-250

[55] *ASM Handbook Committee (2002). ASM Handbook. Friction, Lubrication and Wear Technology*. U.S.A., ASM International. Volume 18.

[56] Rabinowicz, E. (1995). *Friction and Wear of Materials*. New York, John Wiley and Sons.

[57] Bhushan, B. (2012). *Fundamentals of Tribology and Bridging the Gap Between the Macro- and Micro/Nanoscales*. Springer Science & Business Media.